Received: 20 March 2020 | Revised: 11 July 2020 | Accepted: 13 July 2020

DOI: 10.1002/nme.6506

RESEARCH ARTICLE

WILEY

A precise critical time step formula for the explicit material point method

Ruichen Ni | **Xiong Zhang**

School of Aerospace Engineering, Tsinghua University, Beijing, 100084, PR China

Correspondence
Xiong Zhang, School of Aerospace Engineering, Tsinghua University, Beijing 100084, PR China.
Email: xzhang@tsinghua.edu.cn

Summary

The material point method (MPM) combines Eulerian method and Lagrangian method and thus both Lagrangian particle position and interaction between neighboring Eulerian grid cells will affect the simulation stability. However, the original critical time step formula in the standard MPM does not reflect the effect of particle position and neighboring cell interaction on stability and overestimates the critical time step so much that the CFL number has to be very small, even smaller than 0.1, to obtain a stable solution at extreme particle positions. Therefore, in many engineering applications, the standard MPM is very expensive due to the small CFL number. In this article, the effect of particle position and neighboring cell interaction on stability of the explicit MPM is studied. An explicit critical time step formula is obtained based on the system eigenvalues in one dimension, and is then extended to two and three dimensions. For extreme deformation problems, the geometric stiffness matrix is taken into consideration which modifies the sound speed of particles in the critical time step formula. Several tests are performed to verify our formula and show a decrease in amount of time steps used for simulation with our formula comparing with the original formula.

KEYWORDS

critical time step, explicit material point method, neighboring cell interaction, particle positions, stability analysis

1 | INTRODUCTION

Numerical methods for modeling large deformation problems could be classified into Eulerian method, Lagrangian method and hybrid method according to how the computational domain is discretized. To combine the advantages of both Eulerian and Lagrangian methods, Harlow[1,2] proposed the particle-in-cell (PIC) method which discretizes the fluid into Lagrangian particles and computational domain into a uniform Eulerian mesh. Sulsky et al extended the FLIP PIC methods[3,4] from fluid mechanics to solid mechanics and named this method as material point method (MPM).[5,6] The MPM has shown its success in simulating extreme deformation events over two decades, such as hypervelocity impact,[7-10] penetration,[11,12] fracture evolution,[13,14] fluid flow,[15-17] fluid-structure interaction,[18-20] landslide,[21,22] and so on. However, a small CFL number is usually required by the explicit MPM for stability, sometimes even smaller than 0.1, if the critical time step is determined by the formula similar to that used in the finite element method.[23-26] More and more scholars find that the particle distribution will heavily affect the stability of simulations.[24,27-29]

There are a lot of works on the stability analysis of other particle methods[30-33] and cell-crossing error in MPM or its variants.[23,25,34] However, a few studies are conducted to analytically examine the effect of particle position on MPM stability. Belytschko et al[30] presented a unified stability analysis of meshless particle methods by perturbation method in one dimension (1D) and two dimension (2D). Nevertheless, this method requires the second-order derivative of shape function to be bounded which the standard MPM cannot satisfy. Balsara[33] applied the von Neumann stability analysis method to SPH method and Renaud et al[27] also applied the von Neumann stability analysis method to discontinuous Galerkin material point method for hyperbolic problems. However, the von Neumann stability analysis method will be invalid in the standard MPM because of the low accuracy in material point integration. Steffen et al[23] proposed an optimal time step by estimating and balancing space and time errors in MPM. The analysis method of moving-mesh MPM proposed is useful in decoupling different error sources, which will also be used in this article. However, in his work the corresponding parameters in the time step formula are decided by one time-step error with uniform particle distribution so that the effect of particle position has not been taken into consideration. Berzins[35] applied the stability analysis of Spigler and Vianello[36] to MPM and derived a stable time step bound for 1D. However, numerical results in his article show that the formula performs well in GIMP method but underestimates the critical time step in the standard MPM.

The critical time step is determined by the maximum frequency of the discretized system, which can be calculated by the generalized eigenvalue problem of system mass matrix and stiffness matrix. Direct calculation of generalized eigenvalue problem is too time-consuming to be used in explicit MPM simulation. Thus, we need to reduce the degrees of freedom and give an explicit critical time step formula for practical uses. Flanagan and Belytschko[37] proposed a transformation of original eigenproblem to reduce the degrees of freedom in FEM and gave the lower and upper bound of critical time step for the uniform strain elements by Gershgorin's theorem. However, the transformation is only valid for the uniform strain elements which requires only one quadrature point. This method has been applied without the transformation into some particle methods, such as nodal integration method,[31,38] but the Frobenious norm of the strain matrix has to be calculated for all elements. Besides, this method gives the critical time step cell by cell. However, MPM is a hybrid method and the interaction of neighboring grid cells should be taken into consideration due to the convection property of particles in Eulerian step.

The aim of the present work is to propose an explicit critical time step formula for the standard explicit MPM, which takes particle position and interaction of neighboring grid cells into consideration. The explicit critical time step formula is first obtained based on the system eigenvalues for the MPM in 1D, and then extended to 2D and three dimension (3D). It also shows that different MPM schemes [namely, update-stress-last (USL), update-stress-first (USF), and modified update-stress-last (MUSL)] have significant different critical time step values. For extreme deformation problems, the geometric stiffness matrix is taken into consideration which will modify the sound speed of a particle by its stress in the critical time step formula.

The rest of this article is organized as follows. First, the standard explicit MPM scheme is briefly reviewed in Section 2. Then, the reason why von Neumann stability analysis method is invalid is analyzed in detail in Section 3. The detailed derivation of critical time step formulae for USL, USF, and MUSL schemes is presented in Section 4. Several numerical tests are performed to verify our critical time step formulae and compare the simulation performance between the original formula and ours in Section 5. Finally, conclusions and remarks are drawn in Section 6.

2 | MATERIAL POINT METHOD

The weak form equivalent to momentum equation and traction boundary condition in updated Lagrangian (UL) formulation is given as

$$\int_\Omega \rho \ddot{\boldsymbol{u}} \cdot \delta \boldsymbol{u} \mathrm{d}V + \int_\Omega \boldsymbol{\sigma} : \delta \epsilon \mathrm{d}V - \int_\Omega \rho \boldsymbol{b} \cdot \delta \boldsymbol{u} \mathrm{d}V - \int_{\Gamma_t} \bar{\boldsymbol{t}} \cdot \delta \boldsymbol{u} \mathrm{d}A = 0, \tag{1}$$

where Γ_t denotes the traction boundary of material domain Ω, ρ is the current density, $\boldsymbol{u}$ is the displacement, $\boldsymbol{\sigma}$ is the Cauchy stress in the current configuration, ϵ is the strain tensor, $\boldsymbol{b}$ is the body force per unit mass and $\bar{\boldsymbol{t}}$ is the traction on the boundary.

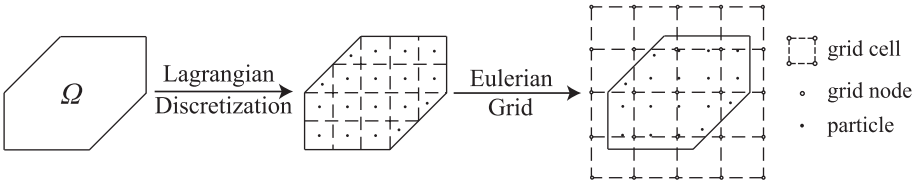

FIGURE 1 Standard MPM discretization. MPM, material point method

2.1 | Standard explicit MPM

The standard MPM discretizes the material domain Ω into a set of Lagrangian particles moving through an Eulerian background grid, as shown in Figure 1. The particles act as quadrature points in calculating the integration of weak form equation, and material density can be approximated with

$$\rho(\boldsymbol{x}) = \sum_{p=1}^{n_p} m_p \delta(\boldsymbol{x} - \boldsymbol{x}_p), \tag{2}$$

where n_p is the total number of particles, m_p is the mass of particle p, δ is the Dirac delta function with dimension of the inverse of particle volume, and $\boldsymbol{x}_p$ is the spatial coordinates of particle p.

The displacement field $\boldsymbol{u}(\boldsymbol{x})$ of the computational domain is interpolated from the grid nodal displacement $\boldsymbol{u}_I$ by the shape function $N_I(\boldsymbol{x})$ of each grid node I, namely

$$\boldsymbol{u}(\boldsymbol{x}) = \sum_{I=1}^{n_g} N_I(\boldsymbol{x}) \boldsymbol{u}_I, \tag{3}$$

where $N_I(\boldsymbol{x})$ is the linear/bilinear/trilinear shape function for standard MPM in 1D/2D/3D as that used in FEM.

Substituting Equations (2) and (3) into the weak form Equation (1) leads to the discrete momentum equation at each grid point

$$\dot{\boldsymbol{p}}_I = \boldsymbol{f}_I^{\text{int}} + \boldsymbol{f}_I^{\text{ext}}, \quad \forall \boldsymbol{x}_I \notin \Gamma_u \tag{4}$$

in which

$$\boldsymbol{p}_I = m_I \dot{\boldsymbol{u}}_I \tag{5}$$

is the momentum at grid point I,

$$m_I = \sum_{p=1}^{n_p} m_p N_I(\boldsymbol{x}_p) \tag{6}$$

is the lumped grid mass matrix,

$$\boldsymbol{f}_I^{\text{int}} = -\sum_{p=1}^{n_p} \nabla N_{Ip} \cdot \boldsymbol{\sigma}_p \frac{m_p}{\rho_p} \tag{7}$$

and

$$\boldsymbol{f}_I^{\text{ext}} = \sum_{p=1}^{n_p} m_p N_{Ip} \boldsymbol{b}_p \tag{8}$$

are the internal and external nodal forces with $\boldsymbol{\sigma}_p = \boldsymbol{\sigma}(\boldsymbol{x}_p)$ being the stress of particle p. In Equation (8), the traction term was omitted for simplicity.

The leapfrog central difference integration scheme is used in the standard explicit MPM, which updates the position at integer time steps and the velocity at integer-plus-a-half time steps as

$$\boldsymbol{u}_I^{n+1} = \boldsymbol{u}_I^n + \Delta t^{n+1/2} \dot{\boldsymbol{u}}_I^{n+1/2}, \tag{9}$$

$$\dot{\boldsymbol{u}}_I^{n+1/2} = \dot{\boldsymbol{u}}_I^{n-1/2} + \Delta t^n \ddot{\boldsymbol{u}}_I^n, \tag{10}$$

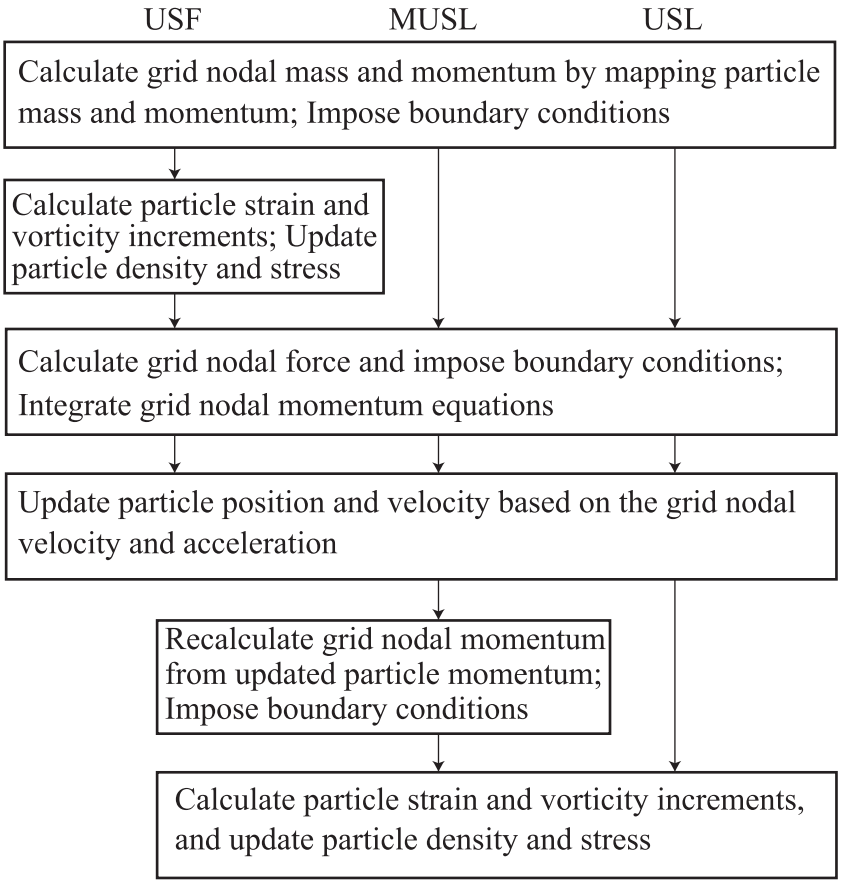

FIGURE 2 Flow chart of different MPM schemes.[6] MPM, material point method

where $\Delta t^{n+1/2} = t^{n+1} - t^n$ and $\Delta t^n = t^{n+1/2} - t^{n-1/2} = \frac{1}{2}(\Delta t^{n-1/2} + \Delta t^{n+1/2})$. $\boldsymbol{u}_I^{n+1}$ and $\boldsymbol{u}_I^n$ denote the displacement vectors at time t^{n+1} and t^n, $\dot{\boldsymbol{u}}_I^{n-1/2}$ denotes the velocity vector at time $t^{n-1/2}$.

The stress state could be updated at the beginning of each time step, or at the end of each time step. The explicit MPM scheme with these two options is referred to as the USF scheme and the USL. In the MUSL scheme, the grid nodal velocity obtained by mapping the updated particle momentum back to the grid nodes is used to update the stress. Different MPM schemes employ different grid nodal velocity fields to update the stress as shown in Figure 2.

2.2 | Moving-mesh MPM

The moving-mesh MPM is referred to an MPM method that is fully Lagrangian, in which the mesh and particles keep stationary in the reference configuration and displacements of both the particles and grid nodes are kept track of. The moving-mesh MPM is actually the same as the standard FEM except that the particles instead of the Gauss points serve as the quadrature points in the moving-mesh MPM. Much more comparisons between standard MPM and moving-mesh MPM were presented by Steffen et al.[23]

The standard MPM computational cycle can be divided into two phases, a Lagrangian phase followed by an Eulerian/convective phase. In the convective phase, the mesh is reset to its original position while the particles are remain in their current positions. The solution on the new grid can be reconstructed from the information carried by the particles, as shown in Figure 2. The reconstruction of the velocity field from particles to grid nodes based on momentum mapping preserves the monotonicity. Thus, the reconstruction phase will not make the MPM scheme unstable, but introduce errors, such as cell-crossing error, into the calculation. The stability is determined by whether the error will be amplified or not in Lagrangian phase. Therefore, the moving-mesh MPM method is employed in our stability analysis to filter out the error produced by the change of particle distribution.

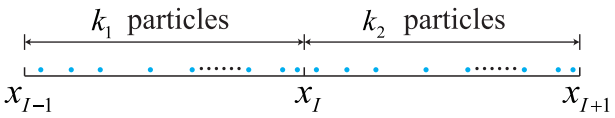

FIGURE 3 Diagram of one-dimension elements and particle distribution [Colour figure can be viewed at wileyonlinelibrary.com]

3 | VON NEUMANN STABILITY ANALYSIS

The von Neumann stability analysis is widely used to determine the critical time step value in finite difference method (FDM), and has been applied in particle methods.[27,33] However, we will show that the Von Neumann stability analysis method is invalid in the standard MPM.

Replacing n by $n-1$ in Equation (9) gives

$$\boldsymbol{u}_I^n = \boldsymbol{u}_I^{n-1} + \Delta t^{n-1/2}\dot{\boldsymbol{u}}_I^{n-1/2}. \tag{11}$$

Eliminating the velocity terms in Equations (9) to (11) leads to

$$\Delta t^{n-1/2}\boldsymbol{u}_I^{n+1} - 2\Delta t^n \boldsymbol{u}_I^n + \Delta t^{n+1/2}\boldsymbol{u}_I^{n-1} = \Delta t^{n-1/2}\Delta t^n \Delta t^{n+1/2}\ddot{\boldsymbol{u}}_I^n. \tag{12}$$

In stability analysis, the external force $\boldsymbol{f}_I^{\text{ext}}$ is assumed to be zero, so the acceleration $\ddot{\boldsymbol{u}}_I^n$ in Equation (12) can be calculated by Equations (4), (6), and (7) as

$$\ddot{\boldsymbol{u}}_I^n = -\frac{\boldsymbol{f}_I^{\text{int}}}{m_I} = -\frac{\sum_{p=1}^{n_p} \nabla N_{Ip} \cdot \boldsymbol{\sigma}_p \frac{m_p}{\rho_p}}{\sum_{p=1}^{n_p} m_p N_{Ip}}. \tag{13}$$

Substituting Equation (13) into Equation (12) leads to

$$[\Delta t^{n-1/2}\boldsymbol{u}_I^{n+1} - 2\Delta t^n \boldsymbol{u}_I^n + \Delta t^{n+1/2}\boldsymbol{u}_I^{n-1}]\sum_{p=1}^{n_p} m_p N_{Ip} + \Delta t^{n-1/2}\Delta t^n \Delta t^{n+1/2}\sum_{p=1}^{n_p} \nabla N_{Ip} \cdot \boldsymbol{\sigma}_p \frac{m_p}{\rho_p} = 0. \tag{14}$$

Equation (14) is valid for all dimensions. Here, we take the 1D problem shown in Figure 3 as an example, in which k_1 and k_2 are the number of particles in the interval $[x_{I-1}, x_I]$ and $[x_I, x_{I+1}]$ individually. The stress of particle p is given by

$$\sigma_p = E\varepsilon_p = E\sum_{I=1}^{n_g} N_{Ip,x} u_I, \tag{15}$$

where E is Young's modulus, ε_p is the strain of particle p, and $n_g = 2$ for linear element in 1D.

With the von Neumann stability analysis method, we assume that the computational domain $x \in [0, L]$ is evenly discretized into S segments

$$\begin{aligned} x_{I+1} - x_I &= x_I - x_{I-1} = h = \frac{L}{S} \\ \Delta t^{n-1/2} &\approx \Delta t^n \approx \Delta t^{n+1/2} \approx \Delta t \end{aligned} \tag{16}$$

and

$$u_I^n = A_n e^{ik_s x}, \tag{17}$$

where A_n is the wave amplitude and

$$k_s = \frac{2\pi}{L}s, \quad s = 1, 2, \ldots, \frac{S}{2}$$

is the wave number related to the spatial discretization.

Equation (14) can be simplified by Equations (15) to (17) as

$$(A_{n+1} - 2A_n + A_{n-1})m_I + \Delta t^2 \cdot A_n \cdot C = 0, \tag{18}$$

where

$$C = \sum_{p=1}^{k_1+k_2} \frac{Em_p}{h^2\rho_p} - \sum_{p=1}^{k_1} \frac{Em_p}{h^2\rho_p} \cdot e^{-ik_s h} - \sum_{p=k_1+1}^{k_1+k_2} \frac{Em_p}{h^2\rho_p} \cdot e^{ik_s h}. \tag{19}$$

Let

$$G = \frac{A_{n+1}}{A_n}, \quad 2t = \frac{C}{m_I}. \tag{20}$$

By substituting Equation (20) into Equation (18), the amplification factor G can be obtained as

$$G = 1 - t \pm \sqrt{(1-t)^2 - 1}. \tag{21}$$

The von Neumann stability condition requires $||G|| \leq 1$, which requires

$$t \in \mathbb{R} \text{ and } 0 \leq t \leq 2, \quad \forall k_s. \tag{22}$$

In the FDM method, the coefficient C could be rewritten into integration form and simplified with the assumption of even spatial discretization in Equation (16) as

$$C = \int_{x_{I-1}}^{x_{I+1}} \frac{E}{h^2}\, \mathrm{d}x - \left(\int_{x_{I-1}}^{x_I} \frac{E}{h^2} e^{-ik_s h}\, \mathrm{d}x + \int_{x_I}^{x_{I+1}} \frac{E}{h^2} e^{ik_s h}\, \mathrm{d}x \right) = \frac{E}{h}(2 - 2\cos(k_s h))$$

so that C is a real number. However, in the MPM method, $\sum_{p=1}^{k_1} m_p/\rho_p \neq h$ and $\sum_{p=k_1+1}^{k_1+k_2} m_p/\rho_p \neq h$ in Equation (19), especially in cell-crossing case. Thus, the coefficient C will become a complex number which violates the requirement in Equation (22). Besides, the constitutive relation in Equation (15) is given in the format of full volume update for derivation while the rate form $\dot{\sigma}_p = E\dot{\varepsilon}_p$ is used in the standard MPM method. The incremental update format of the rate form is $\sigma_p^n = \sigma_p^{n-1} + \sum_{I=1}^{n_g} N_{Ip,x}(u_I^n - u_I^{n-1})$, and the term of σ_p^{n-1} here will lead to a constant term in Equation (18) which will make the amplification factor G difficult to calculate.

In conclusion, the von Neumann stability analysis method is invalid in the standard explicit MPM with central difference integration scheme because of the low accuracy in material point integration and the difficulty in handling the term, σ_p^{n-1}.

4 | CRITICAL TIME STEP DERIVATION

In this section, the explicit formula of the critical time step will be derived based on the system eigenvalues. Homogeneous isotropic material of linear elastic constitutive relation will be applied in the mathematical derivation. The critical stable time step for the central difference integration method, Equations (9) and (10), can be calculated as

$$\Delta t_{\mathrm{cr}} = \frac{2}{\omega_{\max}}, \tag{23}$$

where $\omega_{\max}$ is the maximum angular frequency of the whole system.

Assuming the external force f_{iI}^{ext} to be zero, the momentum equation (4) can be rewritten into vector form as follows

$$\boldsymbol{M}\ddot{\boldsymbol{u}} = \boldsymbol{f}^{\mathrm{int}} \tag{24}$$

in which $\boldsymbol{M}$ is the system mass matrix with the displacements and forces of all the grid nodes being arranged into a vector, such as $\boldsymbol{u} = [u_{11}, u_{21}, u_{31}, \ldots u_{iI} \ldots, u_{1N}, u_{2N}, u_{3N}]^{\mathrm{T}}$ for N grid nodes in 3D. With linear elastic constitutive relation

$\boldsymbol{\sigma} = \boldsymbol{C} : \boldsymbol{\epsilon}$ and the integration formula Equation (7) of the internal forces, the vector $\boldsymbol{f}^{\text{int}}$ can be calculated as

$$\boldsymbol{f}^{\text{int}} = \boldsymbol{K}\boldsymbol{u}, \tag{25}$$

where $\boldsymbol{K}$ is the system stiffness matrix. And $\omega_{\max}$ is the root of the maximum eigenvalue $\lambda_{\max}$ calculated by the generalized eigenvalue problem

$$\boldsymbol{K}\boldsymbol{\phi} = \lambda \boldsymbol{M}\boldsymbol{\phi}. \tag{26}$$

In the following subsections, the USL scheme, MUSL scheme, USF scheme, and sound speed modification will be discussed, respectively.

4.1 | USL scheme

In the UL form, the stress state $\boldsymbol{\sigma}_p$ of particle p is updated as

$$\boldsymbol{\sigma}_p^n = \boldsymbol{\sigma}_p^{n-1} + \boldsymbol{C} : \dot{\boldsymbol{\epsilon}}_p^{n-1/2} \Delta t^{n-1/2}, \tag{27}$$

where the particle strain rate $\dot{\boldsymbol{\epsilon}}_p$ is calculated by the gradient of the velocity field constructed from grid nodes as

$$\dot{\boldsymbol{\epsilon}}_p^{n-1/2} = \frac{1}{2}(\boldsymbol{\nabla}\dot{\boldsymbol{u}}_p^{n-1/2} + \dot{\boldsymbol{u}}_p^{n-1/2}\boldsymbol{\nabla}) = \sum_{I=1}^{n_g}(\boldsymbol{\nabla} N_{Ip}^{n-1})\dot{\boldsymbol{u}}_I^{n-1/2}. \tag{28}$$

Taking the configuration of $n-1$ time step as the current configuration, we have

$$\dot{\boldsymbol{u}}_I^{n-1/2}\Delta t^{n-1/2} = \boldsymbol{u}_{iI}^n - \boldsymbol{u}_{iI}^{n-1} = \Delta \boldsymbol{u}_I, \tag{29}$$

and

$$\dot{\boldsymbol{u}}_I^{n-1/2} = \frac{\mathrm{d}}{\mathrm{d}t}(\Delta \boldsymbol{u}_I), \quad \ddot{\boldsymbol{u}}_I^n = \frac{\mathrm{d}^2}{\mathrm{d}t^2}(\Delta \boldsymbol{u}_I). \tag{30}$$

Substituting Equations (27) to (29) into Equation (7), the internal force can be calculated as

$$\boldsymbol{f}_I^{n,\text{int}} = \boldsymbol{f}_I^{n,\text{geo}} + \boldsymbol{f}_I^{n,\text{mat}}, \tag{31}$$

where

$$\boldsymbol{f}_I^{n,\text{geo}} = -\sum_{p=1}^{n_p}(\boldsymbol{\nabla} N_{Ip}^n)\cdot \boldsymbol{\sigma}_p^{n-1} V_p^n \tag{32}$$

$$\boldsymbol{f}_I^{n,\text{mat}} = -\sum_{p=1}^{n_p}\sum_{J=1}^{n_g}(\boldsymbol{\nabla} N_{Ip}^n)\cdot \boldsymbol{C} : (\boldsymbol{\nabla} N_{Jp}^{n-1}\Delta \boldsymbol{u}_J) V_p^n \tag{33}$$

and the global stiffness matrices can be obtained in submatrix form by the internal nodal forces $\boldsymbol{f}_I^{n,\text{geo}}$ and $\boldsymbol{f}_I^{n,\text{mat}}$, respectively, as

$$\boldsymbol{K}_{IJ}^{n,\text{geo}} = -\frac{\partial \boldsymbol{f}_I^{n,\text{geo}}}{\partial(\Delta \boldsymbol{u}_J)}, \quad \boldsymbol{K}_{IJ}^{n,\text{mat}} = -\frac{\partial \boldsymbol{f}_I^{n,\text{mat}}}{\partial(\Delta \boldsymbol{u}_J)}. \tag{34}$$

The geometric internal force $\boldsymbol{f}_I^{n,\text{geo}}$ in Equation (32) is caused by geometric nonlinearity and will be elaborated in Section 4.3. The element stiffness matrix can be given here by the material internal force $\boldsymbol{f}_I^{n,\text{mat}}$ defined in Equation (33) as

$$\boldsymbol{K}_e^{n,\text{mat}} = \sum_{p=1}^{n_p^e}\boldsymbol{B}_e^{n,\text{T}}\boldsymbol{D}\boldsymbol{B}_e^{n-1} V_p, \tag{35}$$

where $\boldsymbol{B}_e$ is the strain matrix of grid cell e and $\boldsymbol{D}$ is the constitutive matrix.

In the UL form of the explicit MPM scheme, the displacement $\Delta \boldsymbol{u}_I$ is very small because of the small time step value. That is, the difference between the configurations of time step $n-1$ and n is very small. With the assumption of moving mesh MPM that the mesh and particles keep stationary in the reference configuration, we have

$$\boldsymbol{B}_e^n \approx \boldsymbol{B}_e^{n-1}. \tag{36}$$

The greatest difference between MPM and FEM is that the particles instead of the Gauss points serve as the quadrature points which makes the von Neumann stability analysis method invalid. In FEM, Irons has proved that the maximum frequency of the whole system is always smaller than or equal to the maximum frequency of every grid cell. However, in MPM, the cell-by-cell formula will lead to a very small critical time step estimate in some particle distributions while the actual critical time step can be rather large, which will be revealed in details with numerical examples in Section 5. In the standard MPM, the particles will not keep stationary in the reference configuration anymore and cell-crossing frequently occurs in the simulation. So, we need to take the interaction between neighboring grid cells into consideration.

As shown in Figure 3, we assume that the standard MPM has uniform mesh discretization in the 1D computational domain, that is, $x_{I+1} - x_I = x_I - x_{I-1} = h$. Given that the sectional area is A, the Young's modulus is E, and the particles are numbered from 1 to $k_1 + k_2$, the stiffness matrix of the two-cell pair can be calculated as

$$\boldsymbol{K}^{n,\mathrm{mat}} = \begin{bmatrix} K_1^n & -K_1^n & 0 \\ -K_1^n & K_1^n + K_2^n & -K_2^n \\ 0 & -K_2^n & K_2^n \end{bmatrix} \tag{37}$$

in which

$$K_1^n = \frac{AE\sum_{p=1}^{k_1} l_p^n}{h^2}, \quad K_2^n = \frac{AE\sum_{p=k_1+1}^{k_1+k_2} l_p^n}{h^2}, \tag{38}$$

where l_p is the length represented by material particle p.

The lumped mass matrix is always used in the standard explicit MPM for the computational efficiency, that is

$$\boldsymbol{M}^n = \begin{bmatrix} M_{I-1}^n & 0 & 0 \\ 0 & M_I^n & 0 \\ 0 & 0 & M_{I+1}^n \end{bmatrix}, \tag{39}$$

where

$$M_{I-1}^n = \sum_{p=1}^{k_1} m_p N_{(I-1)\ p}^n, \quad M_I^n = \sum_{p=1}^{k_1+k_2} m_p N_{I\ p}^n, \quad M_{I+1}^n = \sum_{p=k_1+1}^{k_1+k_2} m_p N_{(I+1)\ p}^n. \tag{40}$$

By solving the generalized eigenvalue problem $\boldsymbol{K}^{n,\mathrm{mat}}\boldsymbol{\phi} = \lambda \boldsymbol{M}^n \boldsymbol{\phi}$, the maximum eigenvalue can be obtained as

$$\lambda_{\max} = \frac{1}{2}\left\{ K_1^n C_1 + K_2^n C_2 + \sqrt{(K_1^n C_1 - K_2^n C_2)^2 + 4\frac{K_1^n K_2^n}{M_I^n M_I^n}} \right\}, \tag{41}$$

where

$$C_1 = \frac{1}{M_{I-1}^n} + \frac{1}{M_I^n}, \quad C_2 = \frac{1}{M_I^n} + \frac{1}{M_{I+1}^n}.$$

The coefficients M_{I-1},M_I, and M_{I+1} of the lumped mass matrix have already been calculated in the reconstruction step of the standard MPM. However, the coefficients of K_1 and K_2 need to be calculated additionally, which is

time-consuming and difficult to be extended to 2D and 3D. In order to simplify the result, we introduce the inequalities

$$\left(\min_{p=1}^{k_1+k_2}\rho_p^n\right)K_1^n \le \frac{AE\sum_{p=1}^{k_1}\left(\min_{p=1}^{k_1}\rho_p^n\right)l_p^n}{h^2} \le \frac{E\sum_{p=1}^{k_1}m_p}{h^2} = \frac{Em_1}{h^2},$$
$$\left(\min_{p=1}^{k_1+k_2}\rho_p^n\right)K_2^n \le \frac{AE\sum_{p=k_1+1}^{k_1+k_2}\left(\min_{p=k_1+1}^{k_1+k_2}\rho_p^n\right)l_p^n}{h^2} \le \frac{E\sum_{p=k_1+1}^{k_1+k_2}m_p}{h^2} = \frac{Em_2}{h^2}, \tag{42}$$

where

$$m_1 = \sum_{p=1}^{k_1} m_p,\ m_2 = \sum_{p=k_1+1}^{k_1+k_2} m_p$$

are the total mass of all particles located in the interval $[x_{I-1},x_I]$ and $[x_I,x_{I+1}]$, respectively. Substituting Equation (42) into Equation (41) gives

$$\lambda_{\max} \le \frac{E}{2h^2\min_{p=1}^{k_1+k_2}\rho_p^n}\left\{m_1C_1 + m_2C_2 + \sqrt{[m_1C_1 - m_2C_2]^2 + 4\frac{m_1m_2}{M_I^nM_I^n}}\right\}. \tag{43}$$

By substituting Equation (43) into Equation (23), the critical time step can be calculated as

$$\Delta t_{\mathrm{cr}}^{\mathrm{USL}} = \frac{2}{\sqrt{\lambda_{\max}}} \ge \alpha_{\mathrm{USL}}\Delta t_{\mathrm{cr}}^{\mathrm{ori}}, \tag{44}$$

where

$$\Delta t_{\mathrm{cr}}^{\mathrm{ori}} = \frac{h}{\sqrt{E/\left(\min_{p=1}^{k_1+k_2}\rho_p^n\right)}} \tag{45}$$

is the original critical time step used in the standard MPM method, and

$$\frac{8}{\alpha_{\mathrm{USL}}^2} = m_1C_1 + m_2C_2 + \sqrt{[m_1C_1 - m_2C_2]^2 + 4\frac{m_1m_2}{M_I^nM_I^n}}, \tag{46}$$

where α_{USL} is a coefficient factor depending only on particle mass and grid node mass, and can be efficiently calculated.

4.2 | MUSL and USF scheme

The MUSL scheme maps the updated particle momentum back to the grid nodes in order to update the particle stress at the end of every time step, while the USF scheme maps the particle momentum at the beginning of every time step. Therefore, the MUSL and USF schemes are quite similar, and the difference between these two schemes is that the MUSL scheme employs the shape function N_{Ip}^n at time step n to map the particle momentum, while the USF scheme employs the shape function N_{Ip}^{n+1} at time step $n+1$. With the assumption of moving mesh MPM that the mesh and particles keep stationary in the reference configuration, the shape function N_{Ip} remains the same at different time step. That is, there is no difference between the MUSL and USF scheme in the moving mesh MPM.

The nodal force and stress update formula in MUSL scheme is the same as that in USL scheme, Equations (7) and (27), and the main difference is the remapping of velocity field. Thus, the calculation of particle strain is different

$$\dot{\boldsymbol{\varepsilon}}_p^{n+1/2} = \sum_{I=1}^{n_g}\nabla N_{Ip}^n\dot{\bar{\boldsymbol{u}}}_I^{n+1/2} \tag{47}$$

in which

$$\dot{\bar{\boldsymbol{u}}}_I^{n+1/2} = \frac{\sum_{p=1}^{n_p} m_p \dot{\boldsymbol{u}}_p^{n+1/2} N_{Ip}^n}{\sum_{p=1}^{n_p} m_p N_{Ip}^n}, \tag{48}$$

where the velocity $\dot{\boldsymbol{u}}_p^{n+1/2}$ of particle p is the result at the end of time step $n+1/2$.

With the assumption of moving mesh MPM as mentioned above, the shape function N_{Ip} remains the same at different time step. At the beginning of every time step, the reconstruction of the velocity field takes the form of

$$\dot{\boldsymbol{u}}_{I,\text{begin}}^{n+1/2} = \frac{\sum_{p=1}^{n_p} m_p \dot{\boldsymbol{u}}_p^{n+1/2} N_{Ip}^{n+1}}{\sum_{p=1}^{n_p} m_p N_{Ip}^{n+1}}. \tag{49}$$

Comparing Equation (49) with Equation (48) gives

$$\dot{\bar{\boldsymbol{u}}}_I^{n+1/2} = \dot{\boldsymbol{u}}_{I,\text{begin}}^{n+1/2}. \tag{50}$$

Thus, the MUSL scheme and USF scheme will have identical critical time step under the assumption of moving mesh MPM. However, in the standard MPM, USF scheme introduces numerical energy into simulation system which leads to significant increase in total system energy, while MUSL scheme shows good performance in energy conservation. Therefore, the MUSL scheme will be more stable than USF scheme which, however, cannot be reflected in the critical time step formula given with the assumption of moving mesh MPM.

During the time step n, the velocity $\dot{\boldsymbol{u}}_p^{n+1/2}$ of particle p is calculated by the momentum equation as

$$\dot{\boldsymbol{u}}_p^{n+1/2} = \dot{\boldsymbol{u}}_p^{n-1/2} + \Delta t^n \boldsymbol{a}_p, \tag{51}$$

where

$$\boldsymbol{a}_p = \sum_{I=1}^{n_g} \frac{\boldsymbol{f}_I^{n,\text{int}} N_{Ip}^n}{m_I^n}$$

is the acceleration of particle p. Substituting Equation (51) into Equation (48) results in

$$\dot{\bar{\boldsymbol{u}}}_I^{n+1/2} = \dot{\bar{\boldsymbol{u}}}_I^{n-1/2} + \Delta t^n \frac{\boldsymbol{f}_I^{n,\text{eq}}}{m_I^n}, \tag{52}$$

where

$$\boldsymbol{f}_I^{n,\text{eq}} = \sum_{p=1}^{n_p} m_p N_{Ip}^n \boldsymbol{a}_p \tag{53}$$

is the equivalent nodal force, which can be rewritten in vector form as

$$\boldsymbol{f}^{n,\text{eq}} = \boldsymbol{N}^{n,**} \boldsymbol{N}^{n,*\text{T}} \boldsymbol{f}^{n,\text{int}} \tag{54}$$

in which the equivalent nodal force and the original nodal force are arranged into a vector, such as for N grid nodes in 3D $\boldsymbol{f}$=$[f_{11}, f_{21}, f_{31}, \ldots f_{iI} \ldots, f_{1N}, f_{2N}, f_{3N}]^{\text{T}}$, and $\boldsymbol{N}^*$ and $\boldsymbol{N}^{**}$ are the generalized shape function matrices defined by submatrix as

$$\boldsymbol{N}_{Ip}^* = \text{diag}\left(\frac{N_{Ip}}{m_I}, d\right), \quad \boldsymbol{N}_{Ip}^{**} = \text{diag}(m_p N_{Ip}, d),\ I = 1, 2, \ldots, N \text{ and } p = 1, 2, \ldots, n_p, \tag{55}$$

where diag($\cdot, \cdot$) means diagonal matrix and d is the space dimension. For example, $d = 3$ in 3D problems and

$$\text{diag}(m_p N_{Ip}, d) = \begin{bmatrix} m_p N_{Ip} & 0 & 0 \\ 0 & m_p N_{Ip} & 0 \\ 0 & 0 & m_p N_{Ip} \end{bmatrix}. \tag{56}$$

Still, the geometric internal force $\boldsymbol{f}_I^{n,\mathrm{geo}}$ in Equation (32) will be discussed later. Substituting the original material internal force equation $\boldsymbol{f}^{n,\mathrm{mat}} = \boldsymbol{K}^{n,\mathrm{mat}}\Delta\boldsymbol{u}^n$ into Equation (54) leads to the equivalent system stiffness matrix

$$\boldsymbol{K}^{n,\mathrm{mat,eq}} = \boldsymbol{N}^{n,**}\boldsymbol{N}^{n,*\mathrm{T}}\boldsymbol{K}^{n,\mathrm{mat}}. \tag{57}$$

and then the maximum frequency of the whole system can be obtained by solving the generalized eigenvalue problem $\boldsymbol{K}^{n,\mathrm{mat,eq}}\boldsymbol{\phi} = \lambda\boldsymbol{M}^n\boldsymbol{\phi}$.

From the Equations (31) and (53), we can find that with linear shape function the internal nodal force $\boldsymbol{f}_I^{n,\mathrm{int}}$ of grid node I in USL scheme is supported by the two cells joined at node I while $\boldsymbol{f}_I^{n,\mathrm{eq}}$ of grid node I in MUSL scheme is supported by the neighboring four cells. We should use the neighboring four cells in 1D to calculate the critical time step, but unfortunately it cannot give an explicit formula because of the high order in equation $|\boldsymbol{K}^{n,\mathrm{mat,eq}} - \lambda\boldsymbol{M}^n| = 0$. Thus, the two-cell pair is still used as shown in Figure 3, and it will be shown that the difference between the result of two-cell pair formula and that of the whole system eigenvalue is not too large in Section 5.

The material stiffness matrix $\boldsymbol{K}^{n,\mathrm{mat}}$ and lumped mass matrix $\boldsymbol{M}^n$ of the two-cell pair is defined the same as Equations (37) and (39) in USL scheme, and the generalized shape function matrix $\boldsymbol{N}^*$ and $\boldsymbol{N}^{**}$ in 1D problem are defined by linear shape function as

$$\boldsymbol{N}^{*\mathrm{T}} = \begin{bmatrix} \frac{N_{(I-1)\ 1}}{M_{I-1}} & \frac{N_{I\ 1}}{M_I} & 0 \\ \vdots & \vdots & \vdots \\ \frac{N_{(I-1)\ p}}{M_{I-1}} & \frac{N_{I\ p}}{M_I} & 0 \\ \vdots & \vdots & \vdots \\ \frac{N_{(I-1)\ k_1}}{M_{I-1}} & \frac{N_{I\ k_1}}{M_I} & 0 \\ 0 & \frac{N_{I\ (k_1+1)}}{M_I} & \frac{N_{(I+1)\ (k_1+1)}}{M_{I+1}} \\ \vdots & \vdots & \vdots \\ 0 & \frac{N_{I\ p}}{M_I} & \frac{N_{(I+1)\ p}}{M_{I+1}} \\ \vdots & \vdots & \vdots \\ 0 & \frac{N_{I\ (k_1+k_2)}}{M_I} & \frac{N_{(I+1)\ (k_1+k_2)}}{M_{I+1}} \end{bmatrix}, \boldsymbol{N}^{**\mathrm{T}} = \begin{bmatrix} m_1N_{(I-1)\ 1} & m_1N_{I\ 1} & 0 \\ \vdots & \vdots & \vdots \\ m_pN_{(I-1)\ p} & m_pN_{I\ p} & 0 \\ \vdots & \vdots & \vdots \\ m_{k_1}N_{(I-1)\ k_1} & m_{k_1}N_{I\ k_1} & 0 \\ 0 & m_{k_1+1}N_{I\ (k_1+1)} & m_{k_1+1}N_{(I+1)\ (k_1+1)} \\ \vdots & \vdots & \vdots \\ 0 & m_pN_{I\ p} & m_pN_{(I+1)\ p} \\ \vdots & \vdots & \vdots \\ 0 & m_{k_1+k_2}N_{I\ (k_1+k_2)} & m_{k_1+k_2}N_{(I+1)\ (k_1+k_2)} \end{bmatrix}. \tag{58}$$

Solving the generalized eigenvalue problem $\boldsymbol{K}^{n,\mathrm{mat,eq}}\boldsymbol{\phi} = \lambda\boldsymbol{M}^n\boldsymbol{\phi}$ and utilizing the inequalities in Equation (42), the explicit critical time step formula for MUSL scheme can be obtained as

$$\Delta t_{\mathrm{cr}}^{\mathrm{MUSL}} = \frac{2}{\sqrt{\lambda_{\max}}} \geq \alpha_{\mathrm{MUSL}}\Delta t_{\mathrm{cr}}^{\mathrm{ori}} \tag{59}$$

in which $\Delta t_{\mathrm{cr}}^{\mathrm{ori}}$ is the same as that in USL scheme, and

$$\frac{8}{\alpha_{\mathrm{MUSL}}^2} = A + B + \sqrt{(A-B)^2 + \frac{4m_1m_2}{M_I^nM_I^n}\left(\sum_{p=1}^{k_1}N_{Ip}^nC_{I-1}^p + \sum_{p=k_1+1}^{k_1+k_2}N_{Ip}^nC_{I+1}^p - \sum_{p=1}^{k_1+k_2}N_{Ip}^nC_I^p\right)^2}, \tag{60}$$

where

$$\begin{aligned} C_{I-1}^p &= \frac{m_pN_{(I-1)p}^n}{M_{I-1}^n}, \quad C_I^p = \frac{m_pN_{Ip}^n}{M_I^n}, \quad C_{I+1}^p = \frac{m_pN_{(I+1)p}^n}{M_{I+1}^n}, \\ A &= \frac{m_1}{M_{I-1}^n}\left(\sum_{p=1}^{k_1}N_{(I-1)p}^nC_{I-1}^p - \sum_{p=1}^{k_1}N_{(I-1)p}^nC_I^p\right) + \frac{m_1}{M_I^n}\left(\sum_{p=1}^{k_1+k_2}N_{Ip}^nC_I^p - \sum_{p=1}^{k_1}N_{Ip}^nC_{I-1}^p\right), \\ B &= \frac{m_2}{M_I^n}\left(\sum_{p=1}^{k_1+k_2}N_{Ip}^nC_I^p - \sum_{p=k_1+1}^{k_1+k_2}N_{Ip}^nC_{I+1}^p\right) + \frac{m_2}{M_{I+1}^n}\left(\sum_{p=k_1+1}^{k_1+k_2}N_{(I+1)p}^nC_{I+1}^p - \sum_{p=k_1+1}^{k_1+k_2}N_{(I+1)p}^nC_I^p\right). \end{aligned} \tag{61}$$

It shows from Equations (60) and (61) that the coefficient in MUSL scheme not only depends on mass but also relates to the shape function, which will be much more time-consuming than that in USL scheme. But we will illustrate in the numerical tests that the critical time step in MUSL scheme is much larger than that in USL scheme, even over 10 times in some extreme particle positions.

4.3 | Sound speed modification

In this part, the effect of the geometric internal force $\boldsymbol{f}_I^{n,\text{geo}}$ in Equation (32) is taken into account. The treatments of both USL scheme and MUSL scheme are the same, so only the USL scheme is discussed here. As known, the standard MPM shows its power in dealing with extreme deformation problems, and consequently the effect of geometric nonlinearity on simulation stability should be taken into consideration. That is, the stress term at the end of last time step, that is, σ_p^{n-1} in Section 3 which is difficult to handle by the von Neumann stability analysis method, needs to be reflected in our critical time step formula.

As shown in Equation (31), the grid nodal internal force consists of two parts: one is related to the constitutive relation of a certain material and the other is related to the interaction between the current stress state $\boldsymbol{\sigma}_p$ and the geometric deformation. The first part has been studied thoroughly in Sections 4.1 and 4.2, and the second part will be discussed here by its tangential derivative which leads to the geometric stiffness matrix. Belytschko et al[39] gave the derivation from the geometric internal force to the geometric stiffness matrix. We will give a brief description to the derivation first and then use the geometric stiffness matrix to modify our critical time step formulae.

The definition of the geometric internal force $\boldsymbol{f}_I^{n,\text{geo}}$ in integral form is

$$\boldsymbol{f}_I^{n,\text{geo}} = -\int_V \boldsymbol{\nabla} N_I^n \cdot \boldsymbol{\sigma}^{n-1}\, \mathrm{d}V \tag{62}$$

in which $\boldsymbol{\sigma}^{n-1}$ is viewed as a constant for the calculation of current time step n in UL form. With the assumption of moving mesh MPM that the mesh and particles keep stationary in the reference configuration, we have

$$\boldsymbol{\nabla} N_I^n \approx \boldsymbol{\nabla} N_I^{n-1}. \tag{63}$$

In order to calculate the derivative to time, the geometric internal force needs to be rewritten in total Lagrangian form as

$$\boldsymbol{f}_I^{n,\text{geo}} \approx -\int_V \boldsymbol{\nabla} N_I^{n-1} \cdot \boldsymbol{\sigma}^{n-1}\, \mathrm{d}V = -\int_{V_0} \boldsymbol{\nabla}_{\boldsymbol{X}} N_I^{n-1} \cdot \boldsymbol{S}^{n-1} \cdot \boldsymbol{F}^{n-1,T}\, \mathrm{d}V_0, \tag{64}$$

where V_0 is the initial volume, $\boldsymbol{\nabla}_{\boldsymbol{X}} = \left[\frac{\partial}{\partial X_1}, \frac{\partial}{\partial X_2}, \frac{\partial}{\partial X_3}\right]$, $\boldsymbol{S}$ is the second Piola-Krichhoff stress tensor and $\boldsymbol{F} = \frac{\partial \boldsymbol{x}}{\partial \boldsymbol{X}} = \boldsymbol{I} + \frac{\partial \boldsymbol{u}}{\partial \boldsymbol{X}}$ is the deformation gradient. Then with the velocity defined at integer-plus-a-half time steps in leapfrog scheme, the derivative of the geometric internal force to time can be calculated as

$$\dot{\boldsymbol{f}}_I^{n,\text{geo}} \approx -\int_{V_0} \boldsymbol{\nabla}_{\boldsymbol{X}} N_I^{n-1} \cdot \boldsymbol{S}^{n-1} \cdot \dot{\boldsymbol{F}}^{n-1/2,T}\, \mathrm{d}V_0 = -\int_{V_0} \boldsymbol{\nabla}_{\boldsymbol{X}} N_I^{n-1} \cdot \boldsymbol{S}^{n-1} \cdot \left(\frac{\partial \dot{\boldsymbol{u}}^{n-1/2}}{\partial \boldsymbol{X}}\right)^T \mathrm{d}V_0. \tag{65}$$

Substitute Equation (3) into Equation (65) and rewrite the above derivative back into UL form as

$$\dot{\boldsymbol{f}}_I^{n,\text{geo}} \approx -\int_V \boldsymbol{\nabla} N_I^{n-1} \cdot \boldsymbol{\sigma}^{n-1} \cdot (\boldsymbol{\nabla} N_J^{n-1} \dot{\boldsymbol{u}}_J^{n-1/2})^T\, \mathrm{d}V \approx -\int_V \boldsymbol{\nabla} N_I^n \cdot \boldsymbol{\sigma}^{n-1} \cdot \boldsymbol{\nabla} N_J^{n,T} \dot{\boldsymbol{u}}_J^{n-1/2,T}\, \mathrm{d}V. \tag{66}$$

Finally the geometric stiffness matrix can be obtained by substituting Equation (30) into its tangential derivative definition in submatrix form as

$$\boldsymbol{K}_{IJ}^{n,\text{geo}} = -\frac{\partial \boldsymbol{f}_I^{n,\text{geo}}}{\partial(\Delta \boldsymbol{u}_J)} = -\frac{\partial \dot{\boldsymbol{f}}_I^{n,\text{geo}}}{\partial(\mathrm{d}(\Delta \boldsymbol{u}_J)/\mathrm{d}t)} = -\frac{\partial \dot{\boldsymbol{f}}_I^{n,\text{geo}}}{\partial \dot{\boldsymbol{u}}_J^{n-1/2}} \approx \text{diag}(1,d) \cdot \int_V \boldsymbol{G}_I^{nT} \boldsymbol{\sigma}^{n-1} \boldsymbol{G}_J^n\, \mathrm{d}V, \tag{67}$$

where $\boldsymbol{G}_I^n = \left[\frac{\partial N_I^n}{\partial x_1}, \frac{\partial N_I^n}{\partial x_2}, \frac{\partial N_I^n}{\partial x_3}\right]^T$ and $\boldsymbol{\sigma}$ is the Cauchy stress tensor.

In the 1D problem shown in Figure 3, we have

$$d = 1, \quad G_{I-1}^n = \begin{cases} -\frac{1}{l}, x \in [x_{I-1}, x_I] \\ 0, x \in [x_I, x_{I+1}] \end{cases}, \quad G_I^n = \begin{cases} \frac{1}{l}, x \in [x_{I-1}, x_I] \\ -\frac{1}{l}, x \in [x_I, x_{I+1}] \end{cases}, \quad G_{I+1}^n = \begin{cases} 0, x \in [x_{I-1}, x_I] \\ \frac{1}{l}, x \in [x_I, x_{I+1}] \end{cases} \tag{68}$$

Substituting Equation (68) into Equation (67) gives the geometric stiffness matrix for the two-cell pair as

$$\boldsymbol{K}^{n,\text{geo}} = \begin{bmatrix} K_1^{n,\text{geo}} & -K_1^{n,\text{geo}} & 0 \\ -K_1^{n,\text{geo}} & K_1^{n,\text{geo}} + K_2^{n,\text{geo}} & -K_2^{n,\text{geo}} \\ 0 & -K_2^{n,\text{geo}} & K_2^{n,\text{geo}} \end{bmatrix}, \tag{69}$$

where

$$K_1^{n,\text{geo}} = \frac{A\sum_{p=1}^{k_1} \sigma_p^{n-1} l_p^n}{h^2}, \quad K_2^{n,\text{geo}} = \frac{A\sum_{p=k_1+1}^{k_1+k_2} \sigma_p^{n-1} l_p^n}{h^2} \tag{70}$$

and σ_p^{n-1} is the Cauchy stress of particle p at time step $n-1$ in 1D.

Comparing Equations (37) and (69) shows that the material stiffness matrix $\boldsymbol{K}^{n,\text{mat}}$ and the geometric stiffness matrix $\boldsymbol{K}^{n,\text{geo}}$ have the same form. The internal nodal force is calculated by the addition of these two part as

$$\boldsymbol{f}^{n,\text{int}} = \boldsymbol{f}^{n,\text{geo}} + \boldsymbol{f}^{n,\text{mat}} = -(\boldsymbol{K}^{n,\text{geo}} + \boldsymbol{K}^{n,\text{mat}})\Delta\boldsymbol{u}. \tag{71}$$

With the same treatment as in Section 4.1, the final explicit critical time step formula for USL scheme can be obtained as

$$\Delta t_{\text{cr}}^{\text{USL}} = \alpha_{\text{USL}} \Delta t_{\text{cr}}^{\text{mod}}, \tag{72}$$

where

$$\Delta t_{\text{cr}}^{\text{mod}} = \frac{h}{\sqrt{\max_{p=1}^{k_1+k_2}(E + \sigma_p^{n-1})/\rho_p^n}} \tag{73}$$

is the modified critical time step formula by replacing the Young's modulus E with $E + \sigma_p^{n-1}$ to modify the sound speed of every particle p, and the coefficient α_{USL} is of the same definition as in Equation (46).

5 | NUMERICAL EXAMPLES AND DISCUSSION

In this section, three 1D numerical tests are first designed to verify the 1D formulae of USL scheme, MUSL scheme and USF scheme. Then the formulae will be extended to 2D and 3D formulae based on the orthogonality of MPM background mesh, and the results given by extended formulae and directly solving system eigenvalue problem will be compared through a 2D test. Finally, the simulations of 1D string vibration and 2D cantilever vibration are performed to validate our critical time step formulae and compare the simulation performance between the original critical time step formula and ours.

5.1 | Verification tests for 1D formula

As shown in Figure 4, 1D computational domain is discretized into N cells and there is one particle per cell. The parent coordinate ξ of the particles in hollow dot equals zero, which means that they are set at the cell center. The parent coordinate ξ_r of the particle in red circle varies from -1 to 1, which represents different particle positions. And the

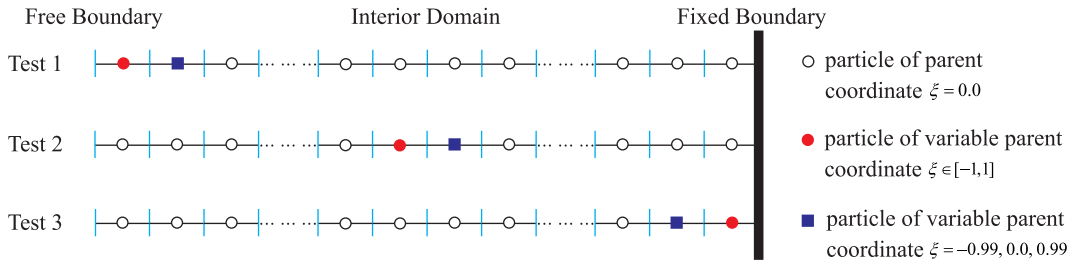

FIGURE 4 Diagram of verification tests for one-dimension formula [Colour figure can be viewed at wileyonlinelibrary.com]

parent coordinate ξ_b of the particle in blue square is chosen from three values, namely, −0.99, 0.0, and 0.99, which is designed to demonstrate the effect of neighboring cell interaction on the critical time step together with the particle in red circle. The two particles in red circle and in blue square are set at different locations, namely, at the free boundary (Test 1), in the interior domain (Test 2), and at the fixed boundary (Test 3), to verify our formulae in different conditions.

The critical time step will be calculated by directly solving the system eigenvalue problem or by the formulae given in Section 4. In order to verify the coefficients in our formulae, the ratio of the critical time step calculated by different methods, $\Delta t_{\text{cr}}^{\text{cal}}$, to that given by the original formula, $\Delta t_{\text{cr}}^{\text{ori}}$, is introduced here

$$R = \frac{\Delta t_{\text{cr}}^{\text{cal}}}{\Delta t_{\text{cr}}^{\text{ori}}}. \tag{74}$$

Thus, the ratio will be not relevant to Young's modulus, material density and spatial discretization precision anymore and be only relevant to particle positions. For critical time step formula, the ratio equals to its coefficient and is easy to calculate. However, for the critical time step of the whole system, we need to solve the generalized eigenvalue problem first, and then the ratio can be obtained by dividing the critical time step with that given by original formula. Thus, we need to give a specific value as Young's modulus $E = 10\ 000$ Pa, material density $\rho = 1.0$ kg/m^3, sectional area $A = 1.0$ m^2, spatial discretization precision $l = 1$ m, and the mass of every particle $m_p = 1.0$ kg to solve the generalized eigenvalue problem.

5.1.1 | USL scheme

In order to illustrate the effect of neighboring cell interaction on the critical time step, 1-cell formula is introduced here to 1D USL scheme by reducing the generalized eigenvalue problem to just one cell $[x_{I-1}, x_I]$

$$\Delta t_{\text{cr}}^{\text{1c,USL}} \geq \Delta t_{\text{cr}}^{\text{mod}} \frac{2}{\sqrt{\frac{m_1}{M_{I-1}} + \frac{m_1}{M_I}}}. \tag{75}$$

Figures 5,6, and 7 plot the ratio R in USL scheme to the parent coordinate ξ_r of the particle in red circle given by directly solving the system eigenvalue problem of the 20-cell system, the 2-cell formula and the 1-cell formula. The two particles in red circle and in blue square are set at the free boundary (Test 1) in Figure 5, in the interior domain (Test 2) in Figure 6 and at the fixed boundary (Test 3) in Figure 7.

In Figure 5A-C, the nodal masses M_{I-1}, M_I, and M_{I+1} used in the formula are partly reconstructed by the particles only located in the interval $[x_{I-1}, x_{I+1}]$, while in Figure 5D-F they are fully reconstructed by all the particles in the supported area, that is, interval $[x_{I-2}, x_{I+2}]$ for linear shape function. The mass of an interior grid node, which is actually large, will be calculated very small when using partly reconstructed nodal masses in some extreme particle distributions, and thus the critical time step value will be severely underestimated. For example, the 2-cell formula gives a very small critical time step value compared with the exact one when the parent coordinate of the particle in blue square equals −0.99 as shown in Figure 5A. When using fully reconstructed nodal masses, the effect of interaction between neighboring 2-cell pairs on the critical time step is taken into consideration and thus the 2-cell formula with fully reconstructed nodal

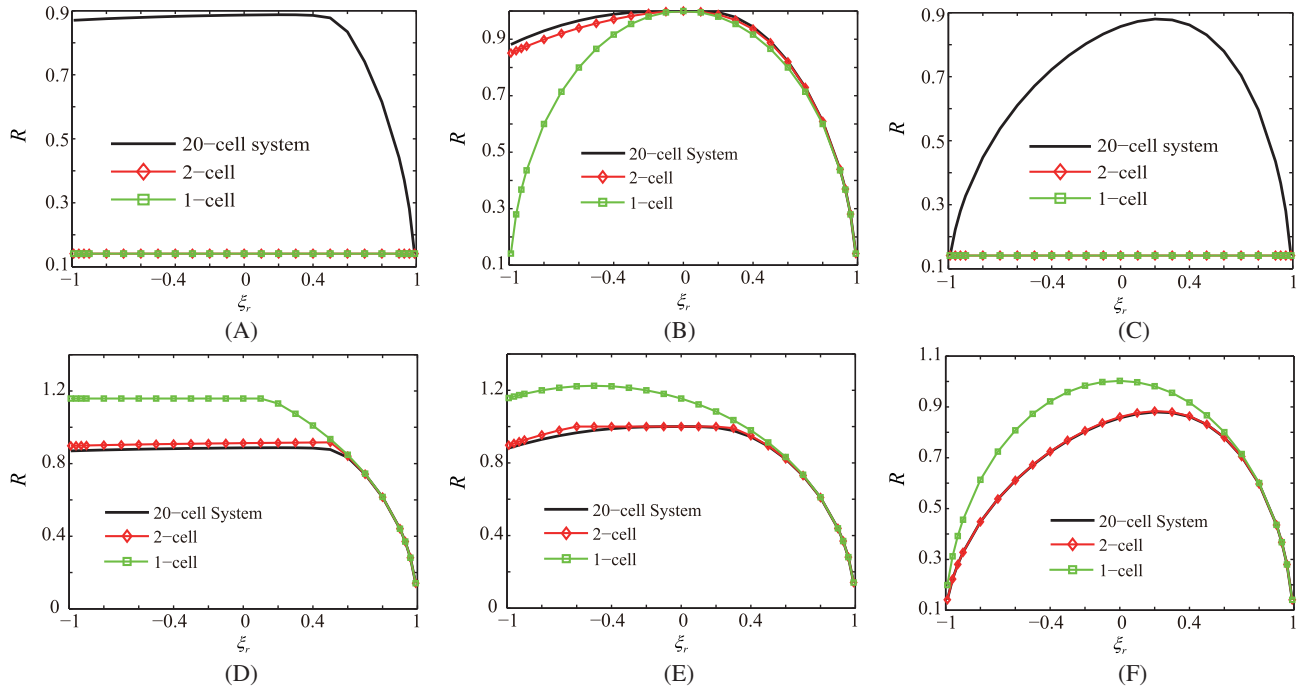

FIGURE 5 The ratio R to the parent coordinate ξ_r of particle in red circle for Test 1 in USL scheme. The parent coordinate of particle in blue square is $\xi_b = -0.99$ in (A) and (D), $\xi_b = 0.0$ in (B) and (E), and $\xi_b = 0.99$ in (C) and (F). Partly reconstructed nodal masses are used in (A) to (C), while fully reconstructed nodal masses are used in (D) to (F). USL, update-stress-last [Colour figure can be viewed at wileyonlinelibrary.com]

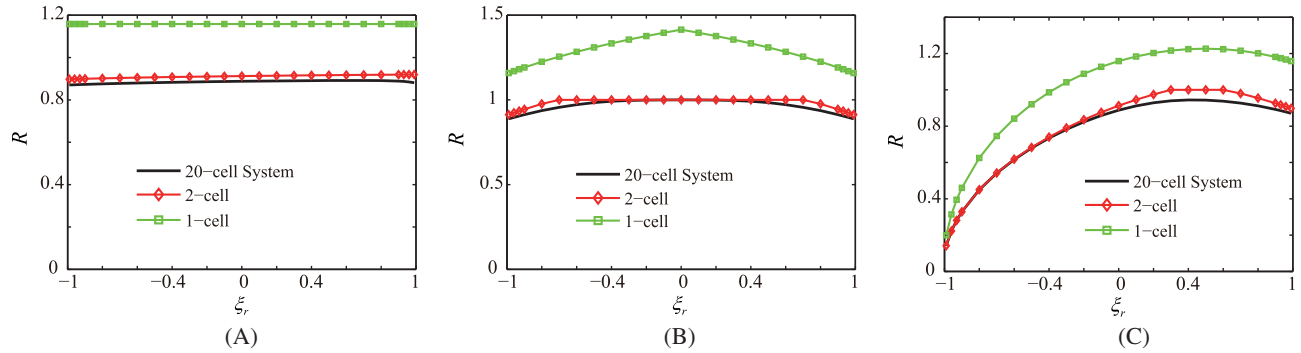

FIGURE 6 The ratio R to the parent coordinate ξ_r of particle in red circle for Test 2 in USL scheme. The parent coordinate of particle in blue square is $\xi_b = -0.99$ in (A), $\xi_b = 0.0$ in (B), and $\xi_b = 0.99$ in (C). USL, update-stress-last [Colour figure can be viewed at wileyonlinelibrary.com]

masses gives a good estimate for the system critical time step in any particle position of Test 1 as shown in Figure 5D-F. Therefore, the fully reconstructed nodal masses M_{I-1}, M_I, and M_{I+1} are used in the 2-cell formula for USL scheme. And thus, we just give the results of our formula with fully reconstructed nodal masses in Figures 6 and 7.

The effect of neighboring cell interaction on the critical time step is revealed here by comparing the results of 2-cell formula and 1-cell formula. As shown in Equation (43) of the maximum system eigenvalue in USL scheme, the neighboring cell interaction is reflected in the term of $4K_1^n K_2^n/(M_I^n)^2$. When just applying the fully reconstructed nodal masses to 1-cell formula, the contribution of the neighboring cell to nodal masses is reflected in the 1-cell formula while the contribution to the element stiffness not, and thus 1-cell formula with fully reconstructed nodal masses overestimates the system critical time step too much to be used in real simulation as shown in Figures 5D-F, 6, and 7. The results of 2-cell formula with fully reconstructed nodal masses and 1-cell formula with partly reconstructed nodal masses are

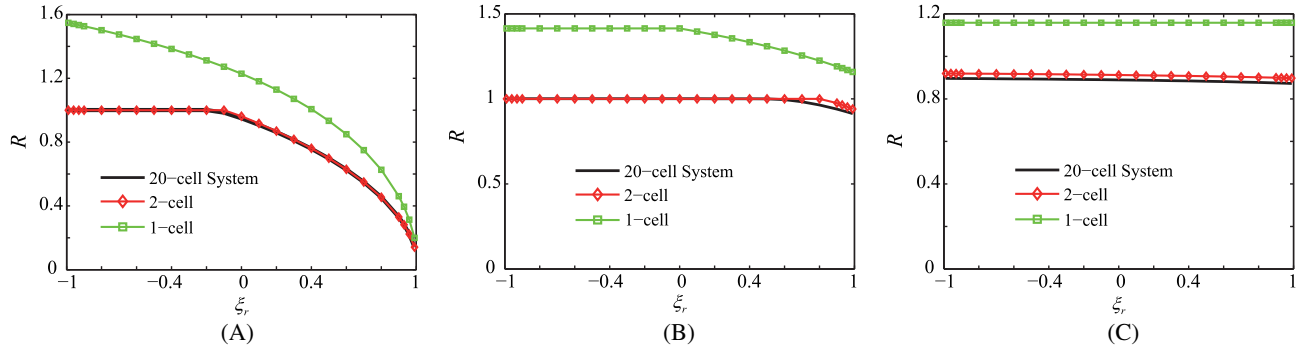

FIGURE 7 The ratio R to the parent coordinate ξ_r of particle in red circle for Test 3 in USL scheme. The parent coordinate of particle in blue square is $\xi_b = -0.99$ in (A), $\xi_b = 0.0$ in (B), and $\xi_b = 0.99$ in (C). USL, update-stress-last [Colour figure can be viewed at wileyonlinelibrary.com]

compared with illustrate the difference between FEM and MPM. In Figure 5B, 1-cell formula gives a much smaller critical time step than the exact one at some particle positions. For example, $\Delta t_{\text{cr}}^{\text{1c,USL}}/\Delta t_{\text{cr}}^{\text{ori}} = 0.14$ while $\Delta t_{\text{cr}}^{\text{exact}}/\Delta t_{\text{cr}}^{\text{ori}} = 0.88$ and $\Delta t_{\text{cr}}^{\text{2c,USL}}/\Delta t_{\text{cr}}^{\text{ori}} = 0.91$ when the parent coordinate of the particle in red circle $\xi_r = -0.99$. In FEM, the density in one cell is uniform and the total mass of the cell is distributed equally to the cell nodes. However, in MPM, the density field has the characteristic of Dirac's function as shown in Equation (2), which leads to a very small nodal mass in the 1-cell formula in extreme particle distributions, such as $M_I = 0.005$ kg in 1-cell formula while $M_I = 0.505$ kg in 2-cell formula when $\xi_r = -0.99$. Thus, the cell-by-cell critical time step proposed by Irons can give a good estimate in FEM but a poor estimate in MPM.

In conclusion, the critical time step will be very small when there exists a very small nodal mass in USL scheme. And, this situation will occur when the material body boundary moves across the cell boundary or fracture happens in the interior of computational domain.

5.1.2 | MUSL and USF scheme

In USL scheme, 1-cell formula is introduced by reducing the generalized eigenvalue problem to just one cell. However, there is no 1-cell formula for MUSL scheme because of the rank deficiency in the generalized shape function matrices, Equation (55). Let us take the uniform particle distribution, for example. Supposing that there is only one particle per cell and all the particles are set at the cell center and of the same mass m_p, we can obtain that the nodal masses M_{I-1} and M_I are equal to the mass of particle m_p and the shape function $N_{(I-1)p}$ and N_{Ip} are both equal to 0.5. Then with the degradation of generalized shape function matrices to one cell $[x_{I-1}, x_I]$ and one particle p in it

$$\boldsymbol{N}^{*} = \begin{bmatrix} \frac{N_{(I-1)\ p}}{M_{I-1}} \\ \frac{N_{I\ p}}{M_I} \end{bmatrix}, \quad \boldsymbol{N}^{**} = \begin{bmatrix} m_p N_{(I-1)\ p} \\ m_p N_{I\ p} \end{bmatrix}, \tag{76}$$

the stiffness matrix can be calculated as

$$\boldsymbol{K}^{\text{eq}} = \boldsymbol{N}^{**} \cdot \boldsymbol{N}^{*T} \cdot \begin{bmatrix} K_1 & -K_1 \\ -K_1 & K_1 \end{bmatrix} = \begin{bmatrix} 0 & 0 \\ 0 & 0 \end{bmatrix}. \tag{77}$$

So, the maximum eigenvalue of $\boldsymbol{K}^{\text{eq}}\boldsymbol{\phi} = \lambda \boldsymbol{M}\boldsymbol{\phi}$ of the 1-cell system with uniform particle distribution equals zero which will give an infinite estimate for the critical time step.

Figure 8 plots the ratio R in MUSL scheme to the parent coordinate ξ_r of particle in red circle given by directly solving the eigenvalue problem of 3-cell system, 5-cell system, 10-cell system and 20-cell system, and the 2-cell formula. Figures 9 and 10 plot the ratio R in MUSL scheme to the parent coordinate ξ_r of particle in red circle given by directly solving the eigenvalue problem of 20-cell system and the 2-cell formula. The two particles in red circle and in blue square are set at

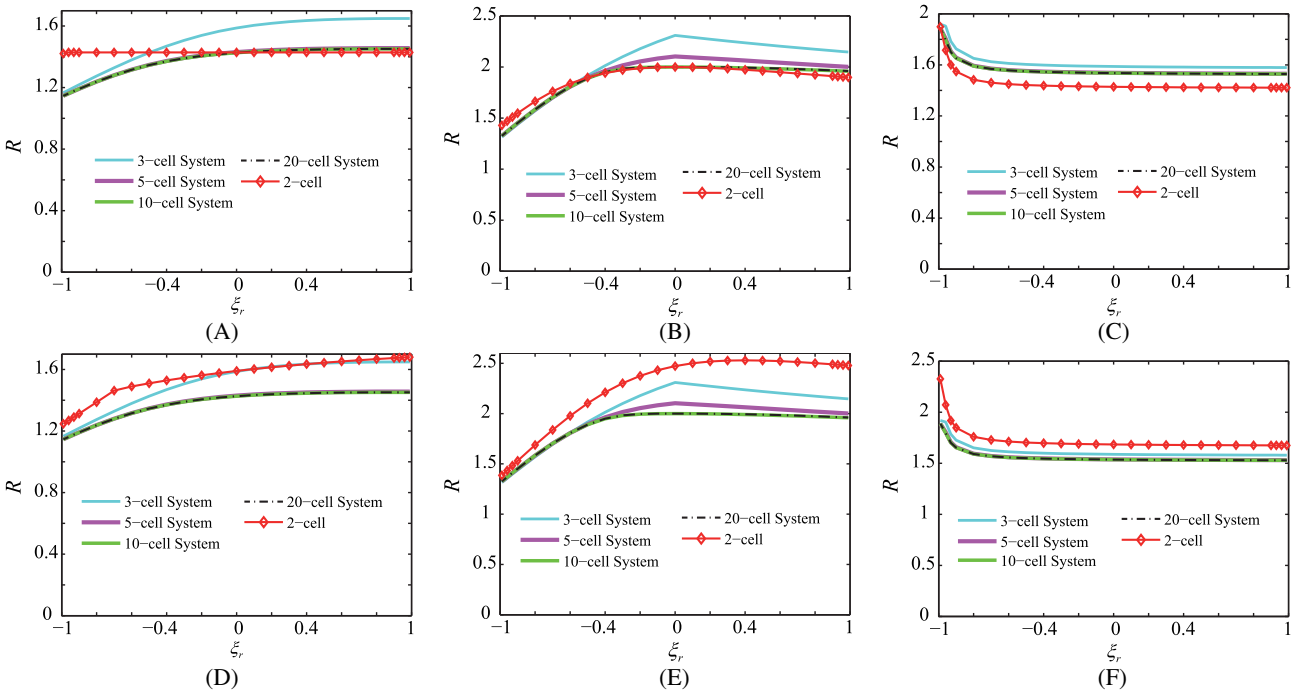

FIGURE 8 The ratio R to the parent coordinate ξ_r of particle in red circle for Test 1 in MUSL scheme. The parent coordinate of particle in blue square is $\xi_b = -0.99$ in (A) and (D), $\xi_b = 0.0$ in (B) and (E), and $\xi_b = 0.99$ in (C) and (F). Partly reconstructed nodal masses are used in (A) to (C), while fully reconstructed nodal masses are used in (D) to (F) [Colour figure can be viewed at wileyonlinelibrary.com]

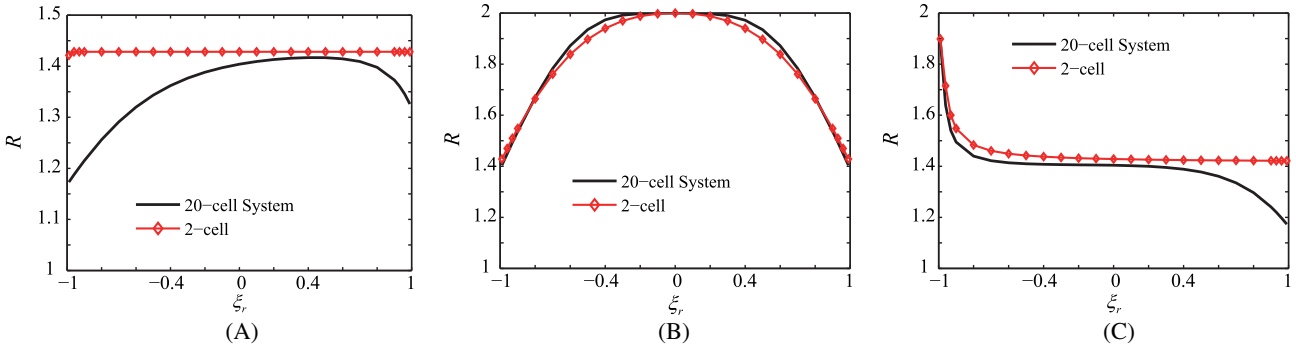

FIGURE 9 The ratio R to the parent coordinate ξ_r of particle in red circle for Test 2 in MUSL scheme. The parent coordinate of particle in blue square is $\xi_b = -0.99$ in (A), $\xi_b = 0.0$ in (B), and $\xi_b = 0.99$ in (C). MUSL, modified update-stress-last [Colour figure can be viewed at wileyonlinelibrary.com]

the free boundary (Test 1) in Figure 8, in the interior domain (Test 2) in Figure 9 and at the fixed boundary (Test 3) in Figure 10.

It has been mentioned in Section 4 that the equivalent internal force, $\boldsymbol{f}_I^{n,\mathrm{eq}}$, of grid node I in MUSL scheme is supported by the neighboring four cells with linear shape function. Therefore, the results of directly solving 3-cell, 5-cell, and 10-cell system eigenvalue problems differ from each other as shown in Figure 8. However, there will be no difference in system critical time step when the cell amount is large enough, such as the results of 10-cell system and 20-cell system. And as shown in Figure 8A-C, the 2-cell formula gives a good estimate for the exact curve, although the effect of enlarged supported area is not reflected in our formula. As a result, it is reasonable to use the 2-cell formula for critical time step calculation in real simulation.

Comparing the results of USL scheme and MUSL scheme, we can find that the ratios in MUSL scheme are all larger than 1.0 at any particle distribution while those in USL scheme are all smaller than 1.0 and even approach to zero at

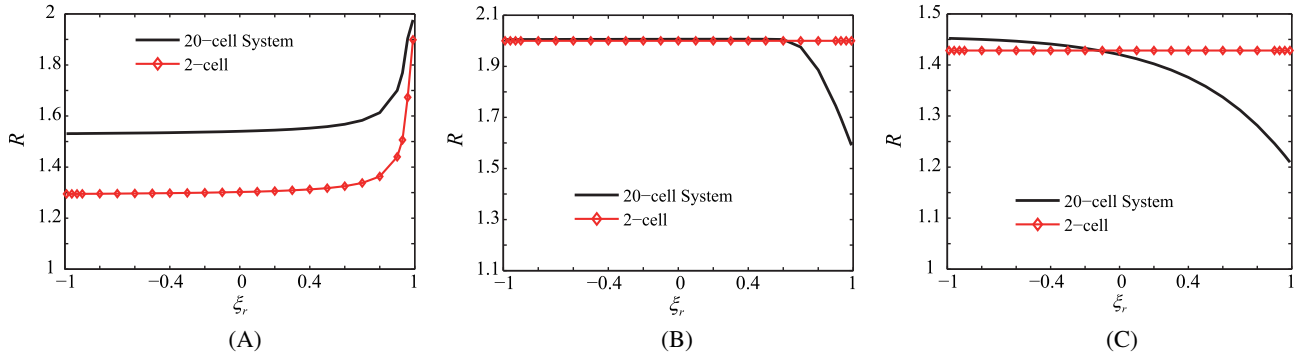

FIGURE 10 The ratio R to the parent coordinate ξ_r of particle in red circle for Test 3 in MUSL scheme. The parent coordinate of particle in blue square is $\xi_b = -0.99$ in (A), $\xi_b = 0.0$ in (B), and $\xi_b = 0.99$ in (C). MUSL, modified update-stress-last [Colour figure can be viewed at wileyonlinelibrary.com]

some extreme particle distributions. In USL scheme, some diagonal elements of the lumped system mass matrix will be an infinitesimal number at those extreme distributions while the system stiffness matrix remains well defined, because the derivative of linear shape function has the characteristic of Heaviside function in the standard MPM. It consequently leads to an infinitesimal critical time step in USL scheme. However, in MUSL and USF scheme, the velocity field of grid nodes is remapped from particles before updating the particle stress, which introduces the generalized shape function matrices as defined in Equation (55) to smooth the system stiffness matrix by Equation (57). Thus, in those extreme particle distributions the system critical time step in MUSL scheme can remain a quite large number, even larger than the value given by the original formula.

The nodal masses M_{I-1}, M_I, and M_{I+1} in Figure 8A-C are partly reconstructed by the particles only located in the interval $[x_{I-1}, x_{I+1}]$, while in 8D-F they are fully reconstructed by all the particles in the supported area, that is, interval $[x_{I-2}, x_{I+2}]$ for linear shape function. The linear shape function N_{Ip} is close to zero when the particle p is near the corresponding cell boundary apart from the cell node I, and the system stiffness matrix is smoothed by the shape function. Therefore, the effect of neighboring cell interaction on the critical time step is eliminated and there is no need to use fully reconstructed nodal masses. As shown in Figure 8, the 2-cell formula with partly reconstructed nodal masses gives a better estimate to the system critical time step than that with fully reconstructed nodal masses. However, the estimation performance of the 2-cell formula in MUSL scheme is worse than that in USL scheme, because the effect of enlarged supported area is not reflected in our formula.

The 2-cell formula gives a good fit to the exact curve of system critical time step when the particle in red circle is located at the free boundary as shown in Figure 8, while it deviates from the exact curve a lot when the particle in red circle is located in the interior domain or at the fixed boundary as shown in Figures 9 and 10. However, those particle distributions of large deviation rarely appear in the physical simulations. For example, the particle distribution of $\xi_r = -0.99$ and $\xi_b = -0.99$ in test 2 represents an isolated particle (the particle in blue square) apart from the other particles. That is, there exists two fracture interface very close to each other, just at a distance of one particle length, which is rare in practical simulation. The 2-cell formula still has a better performance than the original formula in those particle distributions, although a smaller CFL number is needed to guarantee the stability in simulation. Therefore, it is reasonable to use the 2-cell formula in MUSL scheme for physical simulations.

5.2 | Extension to 2D and 3D

The extensions to 2D and 3D in USL scheme, MUSL scheme and USF scheme of the explicit MPM are the same, and thus the extension to 2D in USL scheme is taken here, for example. The background mesh of the standard MPM is structural and orthogonal mesh. An apparent way is to utilize the mesh orthogonality and decouple the calculation of critical time step into x-direction and y-direction. After obtaining the critical time step Δt^x_{cr} and Δt^y_{cr}, respectively, the system critical time step is set to be the smaller one.

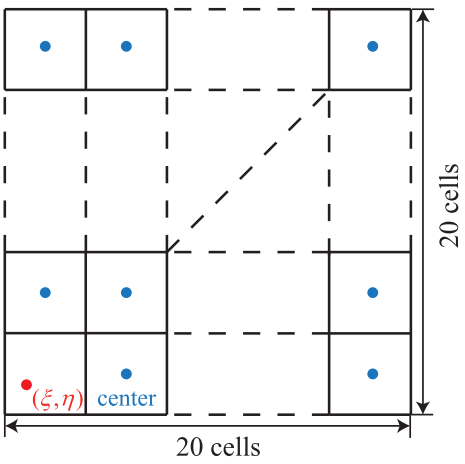

FIGURE 11 Diagram of two-dimension test for the extended formula in USL scheme. USL, update-stress-last [Colour figure can be viewed at wileyonlinelibrary.com]

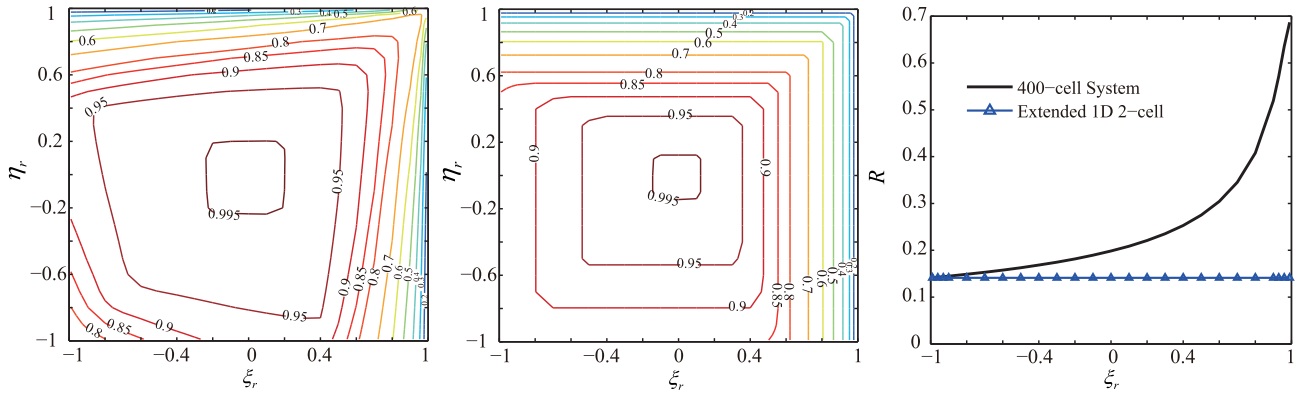

(A) 400-cell System Eigenvalue (B) Extended 1D 2-cell formula (C) Ratio R with respect to fixed $\eta = 0.99$

FIGURE 12 The ratio R to parent coordinates (ξ, η) of red particle in USL scheme. USL, update-stress-last [Colour figure can be viewed at wileyonlinelibrary.com]

Given that two neighboring cells in x-direction are numbered C and $C+1$ and there are k_1 particles in cell C and k_2 particles in cell $C+1$, the formula of Δt^x_{cr} is given by replacing the nodal masses in Equation (46) with the decoupling nodal masses of cell C and $C+1$ in x-direction as

$$M^x_{I-1} = \sum_{p=1}^{k_1} m_p(1-\xi_p), \quad M^x_I = \sum_{p=1}^{k_1} m_p(1+\xi_p) + \sum_{p=k_1+1}^{k_1+k_2} m_p(1-\xi_p), \quad M^x_{I+1} = \sum_{p=k_1+1}^{k_1+k_2} m_p(1+\xi_p) \tag{78}$$

Δt^y_{cr} can be obtained in the same way with the nodal masses calculated by the other parent coordinate η_p.

The 2D test for the extension formula is designed as shown in Figure 11, in which there are 20 cells in each direction and only one particle per cell. The parent coordinates ξ_r and η_r of the red particle range in $[-1, 1]$ which represents different particle positions, and all the blue particles are set to the center of corresponding cell. Figure 12 plots ratio contours to the parent coordinates ξ_r and η_r of the red particle given by solving the 400-cell system eigenvalue problem in Figure 12A and extended 1D 2-cell formula in Figure 12B. Figure 12C plots the ratio, R, to the parent coordinate ξ_r of the red particle with respect to fixed $\eta_r = 0.99$.

As shown in Figure 12, the isohypse remains horizontal or vertical in (B) because of the extension based on mesh orthogonality while the isohypse is oblique in (A). Further comparing the contours of (A) and (B), we can find that the system critical time step is much larger when the red particle is located at the right-top corner with ξ_r and η_r close to 1. It is because that the corresponding diagonal elements of system stiffness matrix and lumped mass matrix will both approach to zero at the same order with the bilinear shape function when the red particle approaches to the right-top cell node. Therefore, there exists an abnormal increase in critical time step when η_r remains 0.99 and ξ_r ranges from -1 to 1 as

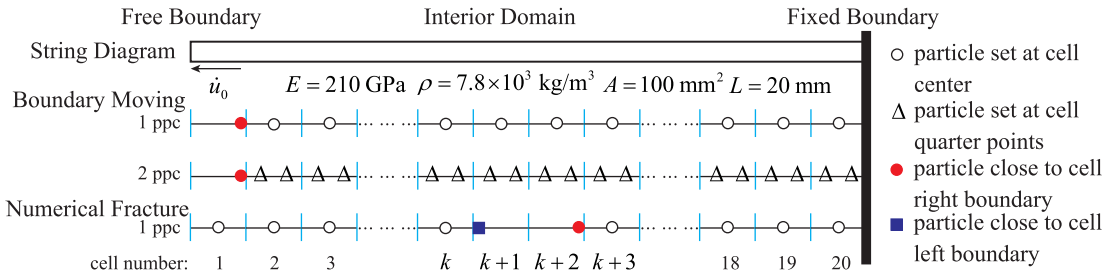

FIGURE 13 Diagram of one-dimension string vibration tests [Colour figure can be viewed at wileyonlinelibrary.com]

shown in subfigure (C). However, the extended 2-cell formula cannot capture this abnormal increase and give a very small critical time step compared with the exact one. Fortunately, not all boundary cells have only one particle at its cell corner and those particles at corner will also move away from the abnormal area in the following steps in simulation. So, we can set aside this abnormal increase phenomenon and just use the orthogonal extended formula for physical simulations.

For 3D extension, the critical time step value in z-direction, Δt^z_{cr}, can be obtained in the same way with the nodal masses calculated by another parent coordinate ζ_p. After obtaining the critical time step Δt^x_{cr}, Δt^y_{cr}, and Δt^z_{cr}, respectively, the system critical time step is set to be the smallest one.

5.3 | 1D string vibration

The tests in previous two subsections 5.1 and 5.2 are all based on moving mesh MPM assumption to verify the 2-cell formula. However, each step of the standard MPM consists of a Lagrangian step and a following Eulerian step. Although the Eulerian step contains only the discard of the old deformed mesh and reconstruction of physical variables to the new mesh which will not cause instability, the interaction between Lagrangian step and Eulerian step will affect the stability characteristic. For example, $\boldsymbol{K}^n_e = \sum_{p=1}^{n^e_p} \boldsymbol{B}^{n,\mathrm{T}}_e \boldsymbol{D} \boldsymbol{B}^{n-1}_e V_p$ is the element stiffness matrix formula in USL scheme. There will be a big difference between $\boldsymbol{B}^n_e$ and $\boldsymbol{B}^{n-1}_e$ when the cell crossing occurs during the time step $n-1$. This instability factor is excluded by the assumption of moving mesh MPM, so we need to validate the applicability of our critical time step formula with some standard MPM simulations. The following tests are all simulated by our laboratory code, MPM3D.

1D string vibration problem has an analytical solution in small deformation which means that the density can be considered as a constant. If the initial velocity condition and boundary conditions are prescribed by

$$\dot{u} = U\frac{\pi}{2L}\sqrt{\frac{E}{\rho}}\sin\left(\frac{\pi}{2L}x + \frac{\pi}{2}\right), \quad \left.\frac{\partial u}{\partial x}\right|_{x=0} = 0, \quad u|_{x=L} = 0, \tag{79}$$

the analytical displacement solution is

$$u = U\sin\left(\frac{\pi}{2L}x + \frac{\pi}{2}\right)\sin\frac{\pi}{2L}\sqrt{\frac{E}{\rho}}t, \tag{80}$$

where U is the amplitude of vibration, E is Young's modulus, ρ is material density and L is total length. In order to satisfy the small deformation assumption, the amplitude U should be set to a small number.

As shown in Figure 13, we set Young's modulus $E = 210$ GPa, material density $\rho = 7.8\times10^3$ kg/m^3, sectional area $A = 100$ mm^2 and total length $L = 20$ mm for simulation. And, the computational domain is discretized into 20 uniform cells of length $l = 1$ mm. The critical time step value will be very small when there exists a very small nodal mass in USL scheme. This situation occurs when the body boundary moves across the cell boundary or fracture happens in the interior of computational domain. Thus, we design two kinds of particle distribution for these two situations, respectively. The tests of 1 particle-per-cell and 2-particle-per-cell in boundary moving situation are used to validate our critical time step formula for different material point discretization precisions. The explicit MPM schemes tested here are moving-mesh MPM, USL scheme, and MUSL scheme.

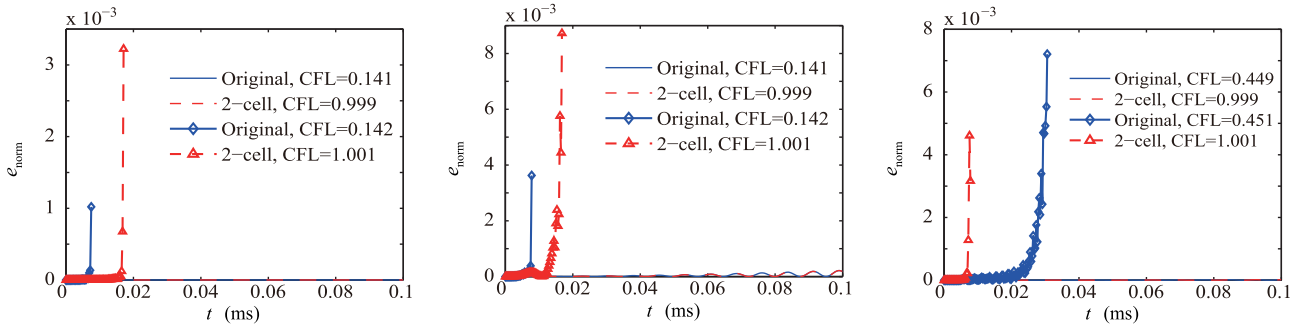

(A) Boundary moving (1 ppc) (B) Boundary moving (2 ppc) (C) Numerical fracture (1 ppc)

FIGURE 14 Time history of L_2 norm of displacement error in moving-mesh MPM. MPM, material point method [Colour figure can be viewed at wileyonlinelibrary.com]

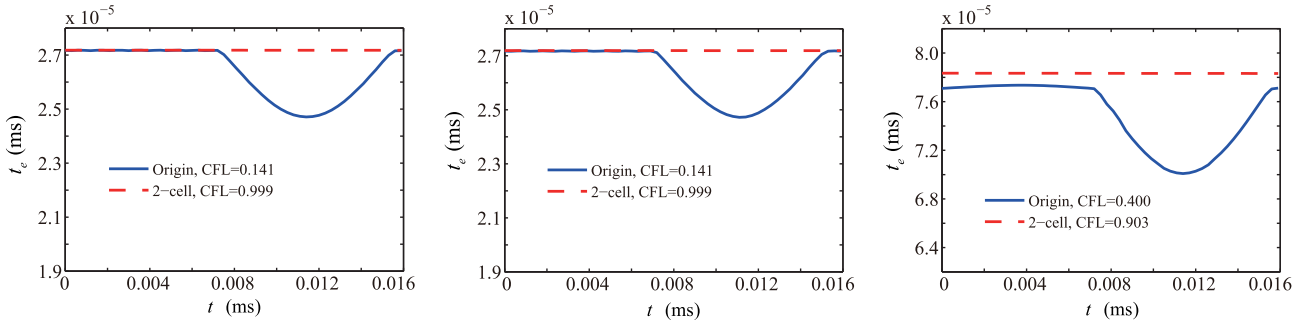

(A) Boundary moving (1 ppc) (B) Boundary moving (2 ppc) (C) Numerical fracture (1 ppc)

FIGURE 15 Time history of critical time step value in 1 vibration cycle (0.016 ms) in moving-mesh MPM. MPM, material point method [Colour figure can be viewed at wileyonlinelibrary.com]

5.3.1 | Moving-mesh MPM

Instability leads to an abrupt increase in error curve at the very beginning of computation while cumulative error leads to low accuracy gradually. Thus, the physical simulation time is chosen to be 0.1 ms which contains about six vibration cycles with the material parameters given. There are two purposes of the moving mesh MPM tests here. One is to verify the correctness of the critical time step calculated by 2-cell formula, while the other is to see the effect of sound speed modification by the stress state of particles. In order to identify the stability characteristic, we introduce the L_2 norm of displacement error as

$$e_{\text{norm}} = \int_{\Omega} (\boldsymbol{u} - \boldsymbol{u}^*) \cdot (\boldsymbol{u} - \boldsymbol{u}^*)\, \mathrm{d}V = \sum_p (\boldsymbol{u}_p - \boldsymbol{u}_p^*) \cdot (\boldsymbol{u}_p - \boldsymbol{u}_p^*) V_p, \tag{81}$$

where $\boldsymbol{u}^*$ is the exact displacement solution and $\boldsymbol{u}_p^* = \boldsymbol{u}^*(\boldsymbol{x}_p)$. The time step size used in each step is determined by

$$t_e = t_{\text{cr}}^{\text{cal}} \cdot \text{CFL} \tag{82}$$

to compare the performance of original formula and 2-cell formula, where $t_{\text{cr}}^{\text{cal}}$ is the critical time step given by different critical time step formulae. Figure 14 plots the time histories of the error norm e_{norm} for small deformation with $U = 2.0$, while Figure 15 plots the time histories of the time step size t_e for large deformation with $U = 815$ to see the effect of sound speed modification. The CFL number used in simulation of each formula is listed in Table 1 together with the amount of total steps used for simulation of physical time 0.1 ms.

As shown in Figure 14, USL scheme with 2-cell formula is stable when CFL number equals 0.999 and unstable when CFL number equals 1.001 for all three tests in small deformation, which means that 2-cell formula gives the exact system

TABLE 1 CFL number and amount of total time steps of different time step formulae for string vibration tests in moving-mesh MPM

Test	Critical time step formula	CFL number used (<1.0)	Total steps for physical simulation time 0.1 ms
Boundary moving (1ppc, $\xi_r = 0.99$)	Original	0.141	3794
	2-cell formula	0.999	3681
Boundary moving (2ppc, $\xi_r = 0.99$)	Original	0.141	3791
	2-cell formula	0.999	3680
Numerical fracture ($\xi_r = -0.8, \xi_b = 0.99$)	Original	0.400(L)/0.449(S)	1337(L)/1156(S)
	2-cell formula	0.903(L)/0.999(S)	1278(L)/1154(S)

Note: (L) means large deformation and (S) means small deformation.
Abbreviation: MPM, material point method.

critical time step value. USL scheme with the original formula is stable when CFL number equals 0.141 and unstable when CFL number equals 0.143, because the original formula does not reflect the effect of particle positions on stability and overestimates the system critical time step too much in extreme particle positions. In conclusion, the 2-cell formula gives a much more accurate estimation for the system critical time step than the original formula.

As shown in Figure 15, the time step size of the original formula is almost the same as that of 2-cell formula in the elongation stage of the string while much smaller than that of 2-cell formula in the compression stage of the string. As mentioned above, the moving mesh MPM is almost the same as FEM except that the material points instead of Gauss points serve as quadrature points. Therefore, the system critical time step given by the original formula is that of smallest element. In the elongation stage of the string, the smallest element is at the fixed boundary which will almost keep the original length because of the small velocity near fixed boundary. In the compression stage, the smallest element is at the free boundary which deforms a lot. Thus, the time step value given by the original formula keeps constant at the elongation stage and decreases a lot in the compression stage. In Section 4.3, the effect of geometric nonlinearity on simulation stability has been taken into consideration and reflected in the 2-cell formula by sound speed modification. The critical time step keeps constant at both the elongation and compression stage due to the sound speed modification. Therefore, the amount of total time steps used for simulation will be smaller with the 2-cell formula than that with the original formula as shown in Table 1.

However, the effect of other nonlinearities on simulation stability has not been considered in our formula, so the CFL number needs to be set smaller than 1.0 in those situations. For example, because the density field has the characteristic of Dirac's function in MPM, the particle distribution in the numerical fracture test represents a nonuniform density field which has drastic changes in the interior of material body due to the extreme particle position as shown in Figure 13. Therefore, the CFL number of 2-cell formula in the numerical fracture test of large deformation is 0.903 as shown in Table 1, which is smaller than 1.0 but acceptable.

5.3.2 | USL scheme

The moving mesh MPM tests have verified the correctness of the critical time step given by 2-cell formula, and this part is to see the difference between the system critical time step based on the moving mesh MPM assumption and the actual critical time step used in the standard MPM. The effect of particle position on stability will also be illustrated here. From the results of 1 ppc and 2 ppc boundary moving tests in moving mesh MPM, we find that there is no difference in the CFL number. Thus, we choose the 1 ppc boundary moving tests here with and without cell crossing. The initial velocity condition of small deformation with $U = 2.0$ is used here.

Figure 16 plots the time histories of the error norm e_{norm} and Figure 17 plots the time histories of the time step size t_e in USL scheme. The CFL number used in simulation of each formula is listed in Table 2 together with the amount of total steps used for simulation of physical time 0.1 ms. The initial parent coordinate, ξ_{r0}, of the particle in red circle is designed to control whether cell crossing occurs or not.

The main difference between the moving mesh MPM and the standard MPM is whether there exists the Eulerian step in each time step cycle or not. Therefore, the difference between the system critical time step based on the moving mesh

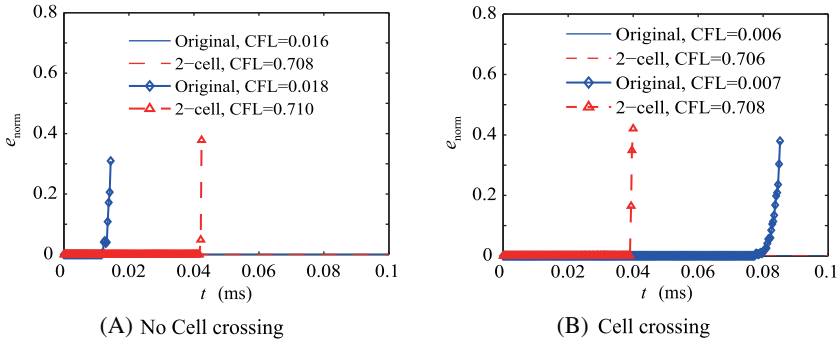

(A) No Cell crossing (B) Cell crossing

FIGURE 16 Time history of L_2 norm of displacement error in USL scheme. USL, update-stress-last [Colour figure can be viewed at wileyonlinelibrary.com]

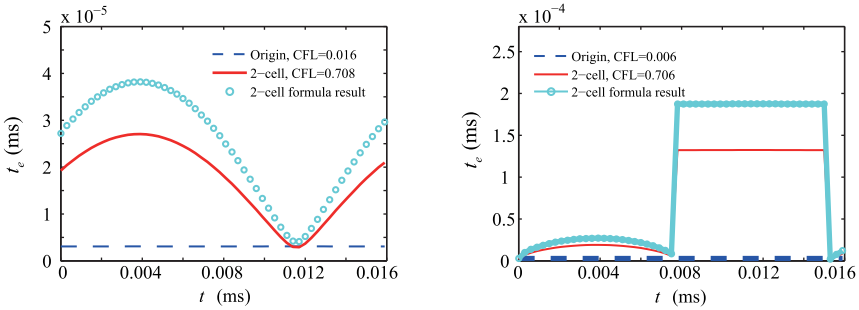

(A) No cell crossing (B) Cell crossing

FIGURE 17 Time history of the critical time step value in 1 vibration cycle (0.016 ms) in USL scheme. USL, update-stress-last [Colour figure can be viewed at wileyonlinelibrary.com]

TABLE 2 CFL number and amount of total time steps of different time step formulae for string vibration tests in USL scheme

Test	Critical time step formula	CFL number used (<1.0)	Total steps for physical simulation time 0.1 ms
Boundary moving, no cell crossing ($\xi_{r0} = 0.99$)	Original	0.016	32 439
	2-cell formula	0.708	8287
Boundary moving, cell crossing ($\xi_{r0} = 0.9999$)	Original	0.006	86 503
	2-cell formula	0.706	4843

Abbreviation: USL, update-stress-last.

MPM assumption and the actual critical time step used in the standard MPM is due to the interaction of Lagrangian step and the following Eulerian step. As shown in Figure 16 and Table 2, the CFL numbers of the 2-cell formula are both about 0.7 whether there exists cell crossing or not. Comparing with the CFL number of 0.999 in moving mesh MPM tests, we can find that the interaction of Lagrangian step and the following Eulerian step will arouse the simulation instability and thus lead to the decrease in the CFL number. Therefore, the CFL number needs to be set about 0.7 for physical simulation by the standard MPM when using the 2-cell formula, which is acceptable.

As shown in Figure 17, the time step size of the original formula almost keeps constant because the length of background cell will not change in the standard MPM and the particle density can be viewed as constant in small deformation problem. The CFL number of the original formula should be set to a very small number, such as 0.016 for no cell crossing and 0.006 for cell crossing in boundary moving tests, so that the time step size given by the original formula can be smaller than or equal to the system critical time step in every step during simulation. However, the ratio of the critical time step of the whole system to that given by the original formula in USL scheme can be infinitely close to zero as shown in Figure 5. That is, the CFL number of the original formula will be infinitely close to zero in some extreme particle distributions, which cannot be acceptable.

The 2-cell formula has a better performance than the original formula due to the much more accurate critical time step given by the 2-cell formula as shown in Figure 17. Table 2 also shows that the total number of time steps used for simulation with the 2-cell formula is about 1/4 of that with the original formula in no cell crossing test, and about 1/17 in cell crossing test.

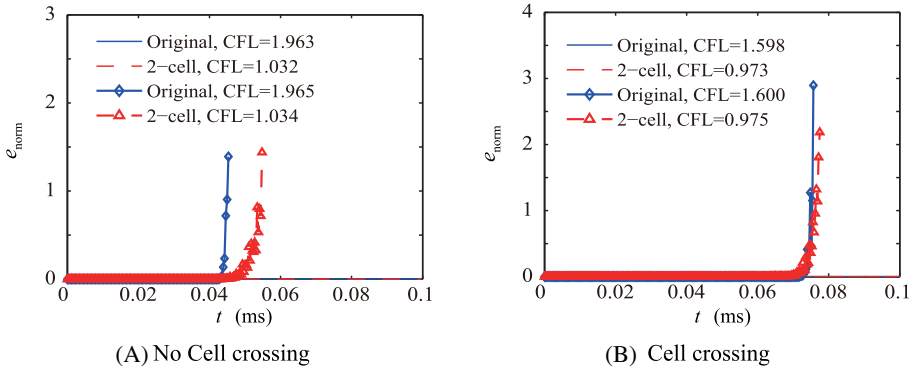

(A) No Cell crossing (B) Cell crossing

FIGURE 18 Time history of L_2 norm of displacement error in MUSL scheme. MUSL, modified update-stress-last [Colour figure can be viewed at wileyonlinelibrary.com]

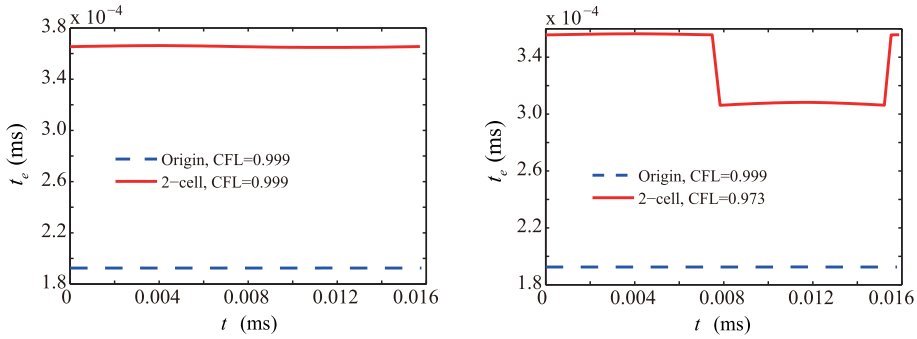

(A) No cell crossing (B) Cell crossing

FIGURE 19 Time history of critical time step value in 1 vibration cycle (0.016 ms) in MUSL scheme. MUSL, modified update-stress-last [Colour figure can be viewed at wileyonlinelibrary.com]

TABLE 3 CFL number and amount of total time steps of different time step formulae for string vibration tests in MUSL scheme

Test	Critical time step formula	CFL number used (<1.0)	Total steps for physical simulation time 0.1 ms
Boundary moving, no cell crossing ($\xi_{r0} = 0.99$)	Original	0.999	520
	2-cell formula	0.999	274
Boundary moving, cell crossing ($\xi_{r0} = 0.9999$)	Original	0.999	520
	2-cell formula	0.973	302

Abbreviation: MUSL, modified update-stress-last.

5.3.3 | MUSL scheme

The stability characteristic of USL scheme and MUSL scheme will be compared in this part. We use the same initial velocity condition of $U = 2.0$ for 1 ppc boundary moving problem as in USL scheme. Figure 18 plots the time histories of the error norm e_{norm} and Figure 19 plots the time histories of the time step size t_e in MUSL scheme. The CFL number used in simulation of each formula is listed in Table 2 together with the amount of total steps used for simulation of physical time 0.1 ms. The critical time step given by original formula or 2-cell formula is supposed to be the maximum time step size used for simulations, and any time step size larger than that should lead to instability. Therefore, the CFL numbers used in performance comparison (listed in Table 3) are required to be smaller than 1.0, although the CFL number of original formula or 2-cell formula may be larger than 1.0 as shown in Figure 18. The initial parent coordinate, ξ_{r0}, of the particle in red circle is designed to control whether cell crossing occurs or not.

As shown in Figure 18, CFL number of 2-cell formula is around 1.0 in MUSL scheme. We have already pointed out the reason why CFL number of 2-cell formula is about 0.7 in USL scheme. However, in MUSL scheme, the remapping step before updating the particle stress will smooth the stiffness matrix, and the smooth weight takes the form of generalized shape function matrices. Although there will still exist a big difference between $\boldsymbol{B}_e^n$ and $\boldsymbol{B}_e^{n-1}$ when the cell crossing occurs during the time step $n-1$, the linear shape function N_{Ip} is close to zero when the particle p is near the corresponding cell boundary apart from the cell node I. Consequently, the effect of interaction between Lagrangian step and the following

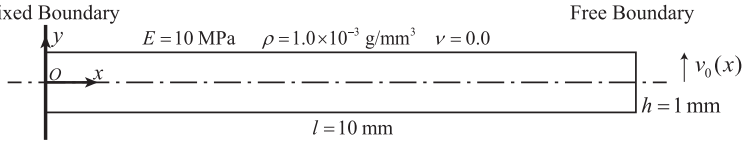

FIGURE 20 Diagram of two-dimension cantilever beam vibration test

Eulerian step will be eliminated by the generalized shape function smoothing. Therefore, CFL number of 2-cell formula can be about 1.0 in MUSL scheme.

Because of the stiffness matrix smoothing, MUSL scheme is much more stable than USL scheme, and the CFL number of the original formula in MUSL scheme could be set to 0.999 while even smaller than 0.1 in USL scheme. Therefore, the benefit in computational efficiency gained from larger critical time step given by the 2-cell formula in MUSL scheme will not be as significant as that in USL scheme. As shown in Table 3, the total number of time steps used for simulation with the 2-cell formula is about 55% of that with the original formula for both no cell crossing test and cell crossing test.

5.4 | 2D cantilever beam vibration

The performance of our critical time step formulae in 1D has been evaluated in the previous tests. And in this section, the 2D cantilever beam vibration test as shown in Figure 20 is presented to evaluate the performance of the extended formula based on mesh orthogonality.

The 2D cantilever beam vibration test has an analytical solution when it satisfies the assumption of Euler-Bernoulli beam, which requires the Poisson's ratio to be zero. If the initial velocity condition and boundary conditions are prescribed by

$$v_0(x) = \omega C \left[\sin(\beta x) - \sinh(\beta x) - \frac{\sin(\beta L) + \sinh(\beta L)}{\cosh(\beta L) + \cos(\beta L)}(\cos(\beta x) - \cosh(\beta x))\right], \tag{83}$$

$$\left.\frac{\partial w}{\partial x}\right|_{x=0} = 0, \quad w|_{x=0} = 0, \quad \left. EJ\frac{\partial^2 w}{\partial x^2}\right|_{x=L} = 0, \quad \left. EJ\frac{\partial^3 w}{\partial x^3}\right|_{x=L} = 0, \tag{84}$$

the analytical displacement solution is

$$w = C\left[\sin(\beta x) - \sinh(\beta x) - \frac{\sin(\beta L) + \sinh(\beta L)}{\cosh(\beta L) + \cos(\beta L)}(\cos(\beta x) - \cosh(\beta x))\right]\sin(\omega t), \tag{85}$$

where C is the amplitude, E is Young's modulus, ρ is material density, L is total length and J is the moment of inertia. The coefficients β, ω and L satisfy the following relationship

$$\beta^4 = \frac{\rho A \omega^2}{EJ}, \quad \cosh(\beta L)\cos(\beta L) + 1 = 0. \tag{86}$$

In order to activate the first mode in cantilever beam vibration, we set β to satisfy the condition $\beta L = 1.875104068711961$ which is the minimum solution of Equation (86). Besides, the amplitude C is set to satisfy the condition $\omega C = 0.1$ mm/s in our test. The background mesh is 12 mm × 2 mm × 0.1 mm, and the discretization precision is 0.1 mm. The boundary condition at $x = 0$ mm is set fixed, and those at $z = 0$ mm and $z = 0.1$ mm are set symmetric while others are free boundaries. Because the Poisson's ratio is zero, the symmetric boundaries at $z-$direction are also valid for the plane stress problem of cantilever beam vibration. The 10 mm × 1 mm × 0.1 mm cantilever beam is uniformly discretized into 8000 material particles which each represents a cubic volume of 0.05 mm × 0.05 mm × 0.05 mm. Given Young's modulus $E = 10$ MPa and material density $\rho = 1.0 \times 10^{-3}$ g/mm^3 as show in Figure 20, the period of cantilever beam vibration can be calculated as 6.19 ms. Thus, the end time of this physical simulation test is set to be 7.0 ms. In the previous 1D tests, CPU time cost for the whole 0.1 ms simulation is very small, and thus CFL number could be tested to the precision of 0.001. However, it is very time-consuming to give a precise CFL number in 2D cantilever beam vibration test, and thus we will use a recommended CFL number according to the CFL number given in the previous 1D tests. The results of recommended CFL number and amount of total time steps used for the whole simulation are listed in Table 4. And pressure contours of different MPM schemes with different critical time step formulae at different simulation time are given in Figures 21 and 22.

MPM scheme	Critical time step formula	Recommended CFL number (<1.0)	Total steps for physical simulation time 7 ms
USL	Original	0.005	Unstable
	2-cell formula	0.7	111 029
MUSL	Original	0.99	7017
	2-cell formula	0.85	6172

Abbreviations: MPM, material point method; MUSL, modified update-stress-last; USL, update-stress-last.

TABLE 4 Recommended CFL number and amount of total time steps used for physical simulation time 7 ms in cantilever vibration test

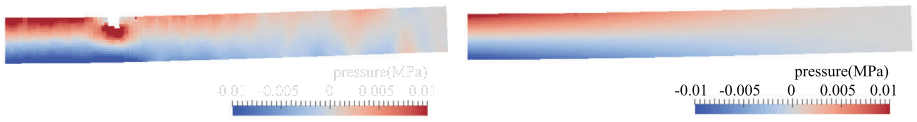

(A) USL, Original, CFL=0.005 (B) USL, 2-cell, CFL=0.70

FIGURE 21 Pressure contour at physical simulation time 1.38 ms in USL scheme. USL, update-stress-last >

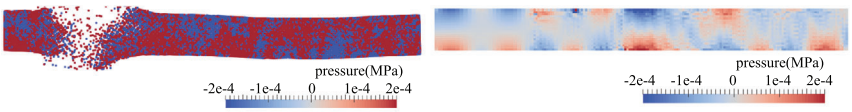

(A) USL, Original, CFL=0.005 (B) USL, 2-cell, CFL=0.70

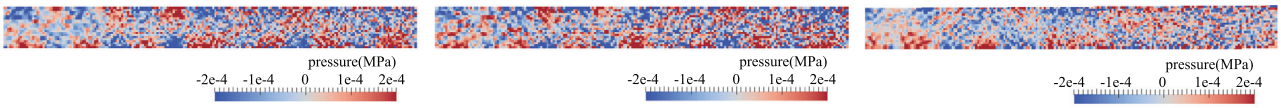

(D) MUSL, Original, CFL=0.99 (E) MUSL, 2-cell, CFL=0.85 (F) MUSL, 2-cell, CFL=0.10

FIGURE 22 Pressure contour at physical simulation time 3.12 ms

Table 4 and Figure 21 show that USL scheme with the original formula is unstable even when CFL number is set to a very small number, such as 0.005. USL scheme with our formulae can be stable at an acceptable CFL number, such as 0.7 for 2-cell formula. The deflection of the whole cantilever beam varies monotonically from zero at $x = 0$ mm to maximum value at $x = 10$ mm. Therefore, the upper boundary at $y = 0.5$ mm or lower boundary at $y = -0.5$ mm of the cantilever beam will intersect the background grid cell boundary when cell crossing occurs, which gives rise to extreme particle distributions. And these extreme particle distributions will lead to a very small critical time step. For example, the smallest time step size in the cantilever beam simulation of USL scheme with 2-cell formula is 4.94×10^{-8} ms and the critical time step given by the original formula equals 9.98×10^{-4} ms, which means that we need to set CFL number smaller than 4.95×10^{-5} to make USL scheme with the original formula stable and the CPU time cost for the whole simulation will be prohibitive.

As shown in Table 4, the MUSL scheme is much more stable than the USL scheme and the total number of time steps used in MUSL scheme is about 1/18 of that used in USL scheme. However, the pressure oscillation in MUSL scheme is much more severe than that in USL scheme, even though we decrease the CFL number to 0.1 in MUSL scheme. From the previous discussion on the generalized shape function matrices, we have known that they will smooth the stiffness matrix and improve the stability in MUSL scheme. However, they also enlarge the supported area used to calculate the grid nodal force and thus lead to severe numerical oscillation in pressure as shown in Figure 22.

6 | CONCLUSIONS

A novel precise critical time step formula is derived for the explicit MPM based on system eigenvalue problem with the assumption of moving-mesh MPM in 1D, and extended to 2D and 3D formulae based on orthogonality of structural Eulerian mesh. The formula has been verified in the standard explicit MPM method with different scheme. The MPM method combines Lagrangian method and Eulerian method, and thus both Lagrangian particle position and interaction between neighboring Eulerian grid cells will affect the stability of MPM method. Besides, the geometric stiffness matrix

is taken into consideration for extreme deformation problem which will modify the sound speed of particle by its stress in the critical time step formula. Several numerical tests have been performed to verify our critical time step formulae and compare the simulation performance between the original formula and ours. USL scheme with the original formula is difficult to be stable even with a very small CFL number, and that with 2-cell formula could be easily stable with an acceptable CFL number, such as 0.7. 2-cell formula could also give a larger stable time step size than the original formula in MUSL scheme. Therefore, the amounts of total time steps in both USL scheme and MUSL scheme with our formulae are smaller than that with the original formula. MUSL scheme is much more stable than USL scheme because of the enlarged supported area used for grid nodal force calculation. However, MUSL scheme suffers lower precision in pressure than USL scheme.

As mentioned above the effect of interaction between Lagrangian step and following Eulerian step in each time step cycle cannot be included with the assumption of moving-mesh MPM. And this is the reason why we need to set CFL number around 0.7 for stability in USL scheme. In MUSL scheme, the 2-cell pair is used to derive the critical time step formula and thus the effect of the enlarged supported area used for grid nodal force calculation on stability is not reflected in our formula. There is a need to address these effects to give a more accurate critical time step in future work.

ACKNOWLEDGEMENT

Supported by the National Natural Science Foundation of China (11672154).

ORCID


Xiong Zhang https://orcid.org/0000-0001-9905-281X

REFERENCES

1. Harlow F.H., Evans M.W.. A machine calculation method for hydrodynamic problems. Tech. Rep. *LAMS-1956*; Los Alamos Scientific Laboratory (1955).
2. Harlow FH. The particle-in-cell computing method for fluid dynamics. *Methods Comput Phys*. 1964;3:319-343.
3. Brackbill JU, Ruppel HM. FLIP: a method for adaptively zoned, particle-in-cell calculations of fluid flows in two dimensions. *J Comput Phys*. 1986;65(2):314-343. https://doi.org/10.1016/0021-9991(86)90211-1.
4. Brackbill JU, Kothe DB, Ruppel HM. Flip: a low-dissipation, particle-in-cell method for fluid flow. *Comput Phys Commun*. 1988;48(1):25-38. https://doi.org/10.1016/0010-4655(88)90020-3.
5. Sulsky D, Chen Z, Schreyer HL. A particle method for history-dependent materials. *Comput Methods Appl Mech Eng*. 1994;118:179-186.
6. Zhang X, Chen Z, Liu Y. *The Material Point Method: A Continuum-Based Particle Method for Extreme Loading Cases*. US: Academic Press; 2016.
7. Gong W, Liu Y, Zhang X, Ma H. Numerical investigation on dynamical response of aluminum foam subject to hypervelocity impact with material point method. *Comput Model Eng Sci (CMES)*. 2012;83(5):527-545.
8. Liu Y, Wang HK, Zhang X. A multiscale framework for high-velocity impact process with combined material point method and molecular dynamics. *Int J Mech Mater Des*. 2013;9(2):127-139.
9. Huang P, Zhang X, Ma S, Wang H. Shared memory openmp parallelization of explicit MPM and its application to hypervelocity impact. *CMES Comput Model Eng Sci*. 2008;38(2):119-148.
10. Ma S, Zhang X, Qiu X. Comparison study of MPM and SPH in modeling hypervelocity impact problems. *Int J Impact Eng*. 2009;36(2):272-282.
11. Huang P, Zhang X, Ma S, Huang X. Contact algorithms for the material point method in impact and penetration simulation. *Int J Numer Methods Eng*. 2011;85(4):498-517.
12. Ma Z, Zhang X, Huang P. An object-oriented MPM framework for simulation of large deformation and contact of numerous grains. *CMES Comput Model Eng Sci*. 2010;55(1):61-88.
13. Liang Y, Benedek T, Zhang X, Liu Y. Material point method with enriched shape function for crack problems. *Comput Methods Appl Mech Eng*. 2017;322:541-562.
14. Cheon Y-J, Kim H-G. An adaptive material point method coupled with a phase field fracture model for brittle materials. *Int J Numer Methods Eng*. 2019;120(8):987-1010. https://doi.org/10.1002/nme.6167.
15. Zhang F, Zhang X, Sze KY, Lian Y, Liu Y. Incompressible material point method for free surface flow. *J Comput Phys*. 2017;330:92-110.
16. Zhao X, Bolognin M, Liang D, Rohe A, Vardon P. Development of in/outflow boundary conditions for MPM simulation of uniform and non-uniform open channel flows. *Comput Fluids*. 2018;179:27-33. https://doi.org/10.1016/j.compfluid.2018.10.007.
17. Zhao X, Liang D, Martinelli M. Numerical simulations of dam-break floods with MPM. *Proc Eng*. 2017;175:133-140. https://doi.org/10.1016/j.proeng.2017.01.041.
18. York AR, Sulsky D, Schreyer HL. Fluid-membrane interaction based on the material point method. *Int J Numer Methods Eng*. 2000;48(6):901-924.
19. Li JG, Hamamoto Y, Liu Y, Zhang X. Sloshing impact simulation with material point method and its experimental validations. *Comput Fluids*. 2014;103:86-99.

20. Liang D, Zhao X, Martinelli M. MPM simulations of the interaction between water jet and soil bed. *Proc Eng*. 2017;175:242-249. https://doi.org/10.1016/j.proeng.2017.01.019.
21. Martinelli M, Rohe A, Soga K. Modeling dike failure using the material point method. *Proc Eng*. 2017;175:341-348. https://doi.org/10.1016/j.proeng.2017.01.042.
22. Fern E, Rohe A, Soga K, Alonso E. *The Material Point Method for Geotechnical Engineering: A Practical Guide*. Boca Raton, FL: CRC Press; 2019.
23. Steffen M, Kirby RM, Berzins M. Decoupling and balancing of space and time errors in the material point method (MPM). *Int J Numer Methods Eng*. 2010;82(10):1207-1243.
24. Renaud A, Heuzé T, Stainier L. A discontinuous Galerkin material point method for the solution of impact problems in solid dynamics. *J Comput Phys*. 2018;369:80-102.
25. Bardenhagen SG, Kober EM. The generalized interpolation material point method. *Comput Model Eng Sci*. 2004;5(6):477-496.
26. Wallstedt PC, Guilkey JE. An evaluation of explicit time integration schemes for use with the generalized interpolation material point method. *J Comput Phys*. 2008;227(22):9628-9642.
27. Renaud A, Heuzé T, Stainier L. Stability properties of the discontinuous Galerkin material point method for hyperbolic problems in one and two space dimensions. *Int J Numer Methods Eng*. 2019;121(4):664-689. https://doi.org/10.1002/nme.6239.
28. Gu YT, Liu GR. Meshless techniques for convection dominated problems. *Comput Mech*. 2006;38(2):171-182.
29. Tran QA, Solowski W. Temporal and null-space filter for the material point method. *Int J Numer Methods Eng*. 2019;120(3):328-360.
30. Belytschko T, Guo Y, Liu WK. A unified stability analysis of meshless particle methods. *Int J Numer Methods Eng*. 2000;48(9):1359-1400.
31. Puso MA, Chen JS, Zywicz E. Meshfree and finite element nodal integration methods. *Int J Numer Methods Eng*. 2008;74(3):416-446.
32. Park CK, Wu CT, Kan CD. On the analysis of dispersion property and stable time step in meshfree method using the generalized meshfree approximation. *Finite Elements Anal Design*. 2011;47(7):683-697.
33. Balsara DS. Von Neumann stability analysis of smoothed particle hydrodynamics–suggestions for optimal algorithms. *J Comput Phys*. 1995;121(2):357-372.
34. Steffen M, Kirby RM, Berzins M. Analysis and reduction of quadrature errors in the material point method (MPM). *Int J Numer Methods Eng*. 2008;76(6):922-948.
35. Berzins M. Nonlinear stability and time step selection for the MPM method. *Comput Particle Mech*. 2018;5(4):455-466.
36. Spigler R, Vianello M. Convergence analysis of the semi-implicit Euler method for abstract evolution equations. *Numer Func Anal Opt*. 1995;5(6):785-803.
37. Flanagan DP, Belytschko T. Eigenvalues and stable time steps for the uniform strain hexahedron and quadrilateral. *J Appl Mech*. 1984;51(1):35-40.
38. Joldes GR, Wittek A, Miller K. Stable time step estimates for mesh-free particle methods. *Int J Numer Methods Eng*. 2012;91(4):450-456.
39. Belytschko T, Liu WK, Moran B. *Nonlinear Finite Elements for Continua and Structures*. Hoboken, NJ: John Wiley and Sons Inc; 2014.

SUPPORTING INFORMATION

Additional supporting information may be found online in the Supporting Information section at the end of this article.

How to cite this article: Ni R, Zhang X. A precise critical time step formula for the explicit material point method. *Int J Numer Methods Eng*. 2020;121:4989–5016. https://doi.org/10.1002/nme.6506